REPORT DOCUMENTATION PAGE

AFRL-SR-BL-TR-99-

0328

1. AGENCY USE ONLY (Leave blank)	2. REPORT DATE	3. REPORT TYPE AND DATES COVERED
	9/30/99	Final Technical Report 7/1/96 - 6/30/99

4. TITLE AND SUBTITLE

DEPSCoR Molecular beam epitaxy of low temperature non-stoichiometric III-V compounds: Theoretical Modeling and Simulation

5. FUNDING NUMBERS

F49620-96-1-0275

6. AUTHOR(S)

Rama Venkat

7. PERFORMING ORGANIZATION NAME(S) AND ADDRESS(ES)

Rama Venkat
Department of Electrical and Computer Engineering
University of Nevada, Las Vegas
4505 Maryland Pkwy., Box 454026
las Vegas, NV 89154-4026

8. PERFORMING ORGANIZATION REPORT NUMBER

N/A

9. SPONSORING / MONITORING AGENCY NAME(S) AND ADDRESS(ES)

Gerald L. Witt
AFoSR/NE
801 N. Randolph Street, Room 732
Arlington, VA 22203-1977

10. SPONSORING / MONITORING AGENCY REPORT NUMBER

Unknown

11. SUPPLEMENTARY NOTES

None

12a. DISTRIBUTION / AVAILABILITY STATEMENT

Unclassified/Distribution Unlimited

12b. DISTRIBUTION CODE

None

13. ABSTRACT *(Maximum 200 Words)*

Surface dynamics dominate the inforporation and segregation of atoms in the molecular beam epitaxy (MBE) of compound semiconductors. A rate equation model is proposed which includes the presence and dynamics of a physisorbed surface layer containing atoms riding the growth surface. The PA layer dictates the incorporation and concentration of various atomic species, such as As^{+}_{Ga} and As^{o}_{Ga} in low temperature GaAs MBE and In in InGaAs MBE growth. Additionally, it influences the RHEED oscillations (ROs) behavior. The model results for the dependence of As^{+}_{Ga} and As^{o}_{Ga} concentrations on beam equivalent pressure (BEP) and growth temperature are in good agreement with experimental data. Using the same kinetic model for the temporal behavior of the surface, the contribution of the PA layer to the RHEED intensity is computed based on kinematical theory of electron diffraction. The experimental observation of the ROs during growth at high and low temperatures with no ROs in the intermediate temperature range of 300-400°C is in good agreement with our model results. The same model is extended to investigate the segregation of In in InGaAs at temperatures in the range of 500-700°C for As (both dimer and tetramer) BEPs of 17 and 36. The model results of In incorporation rate versus growth temperature, segregation coefficient versus growth temperature and desorption rate versus time,are in excellent agreement with various results for a wide range of growth conditions reported in the literature. Activation energies for the various processes are in good agreement with the literature.

14. SUBJECT TERMS	15. NUMBER OF PAGES
MBE Growth, Modeling, LT GaAs, InGaAs	80
	16. PRICE CODE

17. SECURITY CLASSIFICATION OF REPORT	18. SECURITY CLASSIFICATION OF THIS PAGE	19. SECURITY CLASSIFICATION OF ABSTRACT	20. LIMITATION OF ABSTRACT
U	U	U	Ul

Principal Investigator:	Rama Venkat Department of Electrical and Computer Engineering University of Nevada, Las Vegas Las Vegas, NV 89154 Office: (702) 895 1094 Fax: (702) 895 4075
Program Title:	DEPSCOR 95
Proposal Title:	Molecular Beam Epitaxy of Non-stoichiometric III-V Compounds: Theoretical Modeling and Simulation
Grant Number:	F49620-96-1-0275
Project Period:	1 June 1996- 30 July 1999
Report Period:	1 June 1996- 31 July 1999
AFOSR Program Manager:	Dr. Gerald L. Witt Physics and Electronics Electronic Devices, Components and Circuits

Abstract

Surface dynamics dominate the incorporation and segregation of atoms in the molecular beam epitaxy (MBE) of compound semiconductors. A rate equation model is proposed which includes the presence and dynamics of a physisorbed surface layer containing atoms riding the growth surface. The PA layer dictates the incorporation and concentration of various atomic species, such as $As^{+}_{Ga}$and As^{0}_{Ga} in low temperature $GaAs$ MBE and In in $InGaAs$ MBE growth. Additionally, it influences the RHEED oscillations (ROs) behavior. The model results for the dependence of $As^{+}_{Ga}$and As^{0}_{Ga} concentrations on beam equivalent pressure (BEP) and growth temperature are in good agreement with experimental data. Using the same kinetic model for the temporal behavior of the surface, the contribution of the PA layer to the RHEED intensity is computed based on kinematical theory of electron diffraction. The experimental observation of the ROs during growth at high and low temperatures with no ROs in the intermediate temperature range of 300-400°C is in good agreement with our model results. The same model is extended to investigate the segregation of In in $InGaAs$ at temperatures in the range of 500-700 C for As (both dimer and tetramer) BEPs of 17 and 36. The model results of In incorporation rate versus growth temperature, segregation coefficient versus growth temperature and desorption rate versus time, are in excellent agreement with various results for a wide range of growth conditions reported in the literature. Activation energies for the various surface processes are in good agreement with literature.

TABLE OF CONTENTS

LIST OF FIGURES

CHAPTER 1

INTRODUCTION

Molecular beam epitaxy (MBE) is a versatile film growth technique for growing thin epitaxial structures made of semiconductors, metals or insulators. In this technique, the atomic or molecular beams are thermally evaporated onto a heated substrate in an ultra-high vacuum. The ultra-high vacuum allows monitoring of the growth with $in-situ$ tools like reflection high-energy electron diffraction (RHEED). There has been great interest in the past in understanding the properties of low-temperature-grown $GaAs$ (LT-GaAs) grown by MBE at substrate temperatures of 200-400°C, generally followed by annealing at a higher temperature. The material is highly non-stoichiometric with a large excess As incorporated into $GaAs$ in the form of point defects. When annealed at a temperature above 500°C, the material becomes semi-insulating [1] crystal if the thickness is limited to a critical value, with the excess As precipitating to form semi-metallic clusters [2] and the lattice mismatch of the substrate vanishes. The semi-insulating property is an important technological innovation observed first in 1978 since it is useful for fabrication of devices, such as semi-insulating buffer layers for $GaAs$ metal-semiconductor field-effect transistors (MESFET) to eliminate the problem of side-gating [3] and for ultra-high photo-detectors. The point defects are present in the form of antisites arsenic, As_{Ga}, arsenic interstitials, As_i [4] and gallium vacancies, V_{Ga} [5] causing the epilayer to dilate [4]. Of the point defects, As_{Ga} is accepted as the dominant defects [6]. The amount of excess arsenic can be controlled with the substrate temperature and beam equivalent pressure (BEP) during MBE. A considerable amount of As_{Ga} is in the positively charged

state [7] and hence antisites are distinguished as neutral, As^0_{Ga} and charged, As^+_{Ga}, antisites. To maintain the charge neutrality of the material, gallium vacancies are present as triple acceptors, V^{3-}_{Ga}. The ultra-fast trapping characteristics of carriers in these materials which are useful for photo-switching applications have been correlated to the presence and concentration of As^+_{Ga} [8]. It is shown that doping the material with Be increases the As^+_{Ga} concentration from 10% to more than 50% to develop a thermally stable $GaAs$ with sub-picosecond lifetimes [9]. A stochastic model of growth has been utilized to investigate the LT MBE $GaAs$ growth [10]. In the study, a weakly bound physisorbed As (PA) layer is included whose dynamics is essential to explain the experimental observation of temperature and BEP dependencies of As_{Ga} concentration. This study did not include the incorporation of gallium vacancies, V_{Ga} and charged antisites, As^+_{Ga}.

RHEED oscillations (ROs) observed during MBE growth are periodic step density oscillations corresponding to monolayer deposition time [11-14]. ROs have been observed only at high temperatures around 600°C with an As_4 to Ga flux ratio of at least 5:1 until recently when Ibbetson *et al* [15] observed at low temperatures as low as 200°C under strict stoichiometric conditions. In a subsequent Monte Carlo study [16], they suggested that even with very small surface migration rate for Ga, one can achieve enough step density oscillations to obtain ROs. Venkatasubramanian *et al* [17] used a stochastic model of growth allowing for a physisorbed layer of As. It was shown that the ROs were enhanced by the temporal oscillations of the PA layer coverage which exposed the crystal periodically to RHEED beam. Recently, Shen *et al* [18] have shown that stoichiometric condition is not a prerequisite for the RO observation and that the ROs can be observed over a wide range of BEP ratios and temperatures. They also observed that the ROs are suppressed over a temperature window at a fixed BEP and over a BEP ratio window at a fixed temperature.

Indium is observed to segregate to the growth surface during MBE growth of $InGaAs$ [19-35]. The segregation rate is found to be dependent on the As overpressure, substrate temperature and molecular species of arsenic, i.e., As_2 or As_4 [19]. It is found that In segregation is smaller for lower temperature, high As overpressure and As_2 [19]. Additionally, it is observed that the In desorption in the presence of As and Ga fluxes and no In flux, is found to have two desorption mechanisms, one from the surface riding In layer and the other from the crystal surface.

The aim of this work is to modify the stochastic model [10] to make it a comprehensive model which will capture not only the physics of antisite arsenic incorporation and the RO behavior in LT $GaAs$ growth, but also In segregation and desorption in $InGaAs$ growth. Additionally the model shall include both neutral and charged As_{Ga} incorporation. The results of the model will be compared to various experimental results [8,9,15,18,19,21,26,36]. Then the model will be employed to theoretically study the growth mechanisms and to identify the dominant mechanism which controls the incorporation of As^0_{Ga} and As^+_{Ga} and also the behavior of the specular ROs as a function of growth conditions, specifically the influences of growth parameters such as temperature, flux ratio and growth rate. Additionally, the model will be extended to study the In segregation and desorption in $InGaAs$ MBE growth.

1.1 Organization of the Report

A brief overview of MBE of LT GaAs and InGaAs is presented in chapter 2. The details of rate equation model developed to study the antisite incorporation and ROs in the LT MBE In segregation and desorption in InGaAs growth is presented in chapter 3. The details of the surface mechanisms and the formulation of the kinetic rate equation model are presented in section 3.1. The computational details are in sections 3.2. Results and discussions are presented in chapter 4.

CHAPTER 2

OVERVIEW

Crystal growth technology is one of the fast advancing fields related to fabrication of integrated circuits in the recent years. Epitaxy is a growth process of a solid film on a crystalline substrate in which the atoms of the growing film mimic the crystalline arrangement of the atoms of the substrate. Hence, the epitaxially grown layer, usually, exhibits the same crystal structure and the same orientation as the substrate. By present day epitaxial growth techniques, layers of the order of $5\mathring{A}$ to 20 μm of single crystal material can be deposited upon the surface of a single crystal substrate. The development and production of the next generation of high speed discrete and IC devices is inextricably linked to the ability to grow highly complex device structures epitaxially. MBE is distinguished from other vacuum deposition techniques because of its significantly more precise control of the beam fluxes and growth conditions and hence the composition and the thickness of the epilayers. MBE, used at first for studying semiconductor surfaces [37], now has found practical applications in the fabrication of conventional and novel ultrafast quantum devices. The low growth rate of 1μm/hr. ($\approx$1 monolayer/sec.) at low temperatures and ultra high vacuum conditions (UHV) ensures accurate control of stoichiometry, crystallinity, layer thickness and interface abruptness to the level of interatomic dimensions. It is also possible to grow artificial crystals with periodic variation in compositions which are not available in nature. Exploiting the unique advantage of UHV conditions, the growth is controlled *in-situ* by surface diagnostic methods such as RHEED, Auger Electron Spectroscopy (AES) and Scanning Tunneling Microscopy (STM). These powerful analytical tools

for control and analysis enable the fabrication of sophisticated device structures using MBE. Epilayers of many materials have been grown by MBE. But III-V semiconductor compounds, in general, and $GaAs$, in particular, have received the most attention [38]. Of interest to this thesis work is the MBE growth of low temperature (LT) $GaAs$. The experimental and theoretical studies on LT GaAs are summarized in this section.

2.1 Molecular Beam Epitaxy

MBE is a sophisticated crystal growth process in which molecular beams of constituent elements of the epilayer flow towards the heated substrate under ultra high vacuum levels of the order of 10^{-8} Torr. The molecular beams are generated under UHV conditions normally from Knudsen-effusion-cells containing the constituent elements whose temperatures are accurately controlled to enable a good flux stability. Computer controlled, temperatures of the substrate and each of the sources, and operation of shutters dictate the desired chemical composition and doping of the epitaxial films. The molecules of different species of beams have no collisions or interactions before reaching the surface of the substrate as the mean free path of the molecules is very long. Epitaxial growth occurring on the substrate surface involves a series of surface processes like adsorption of the atoms on the substrate surface, surface migration of the adsorbed atoms, incorporation of the atoms into the crystal lattice and thermal desorption of the species. The crystal surface has crystal lattice sites created by the surface dangling bonds and is characterized by its individual chemical activity. The surface processes are characterized by relevant kinetic parameters. The flux of the incoming species is the number of atoms or molecules impinging on an unit area of the surface per second. Not all the atoms arriving at the surface stick to the surface by condensation. The ratio of number of atoms adhering to the surface

to the number of atoms arriving there is called sticking coefficient of the species.

Though MBE growth of II-VI and IV-IV semiconductor compounds as well as of metals, insulators and Si is common, the growth of III-V materials and structures has become more important because of the superior high frequency properties and unique optical properties of the III-V semiconductors as compared to Si. Good compositional control of the growing alloy film is achieved by supplying excess group V species and adjusting the flux densities of the impinging group III beams. Thermal stability of the less stable of the two III-V compounds limits the growth of ternary III-III-V alloys by MBE. At high temperatures, preferential desorption of the more volatile group III element occurs. Thus, the surface composition of the alloy reflects the relative flux ratio of the group III elements only, if the growth is carried out at temperatures below which $GaAs$ is thermally stable [39]. The growth rate is determined almost by the flux rate of group III element.

The group III elements produce monoatomic beams, whereas, the group V elements usually produce dimers or tetramers [40]. The established growth models are not unique to $GaAs$ but valid for other binary III-V compounds such as $AlAs$ [37] and InP [41]. *In-situ* doping of the material is possible. Typically, for III-V compounds, Be is used for p-type doping and Si for n-type. The typical conditions for MBE of high-quality GaAs are a substrate temperature of 600°C, a beam equivalent pressure (BEP) ratio of 15-20, and an extremely low growth rate of 1μ m/hr. [37]. The BEP is the ratio of the flux of the group V element *i.e.*, As to the flux of the group III element *i.e.*, Ga. The BEP is measured with an ion gauge at the growth position. With the Ga effusion furnace at a temperature near 900°C to obtain a 1μm/hr. growth rate, every Ga atom that impinges on the substrate at a temperature of 600°C has enough thermal energy to find a lattice site. The arsenic molecules, originating from an effusion furnace at a temperature of about 250°C, will only result in the incorporation

of an arsenic, As, atom if there is a surface Ga atom to bond to. This results in the growth of stoichiometric material. The possibility of growing high-quality epitaxial layers of different materials on lattice mismatched semiconductor substrates is a topic of considerable interest in MBE for many years. The range of useful devices available with a given substrate is considerably enhanced by this method.

The growing surface is accessible to observation using powerful real-time surface-science diagnostics which require high-vacuum. Hence RHEED is routinely used to monitor the crystal structure and microstructure of growing surfaces. Reflection mass spectrometry (REMS) and modulated beam mass spectrometry (MBMS) are used to monitor the chemistry of growing surfaces, and reflectance difference spectroscopy (RDS) is used to monitor the composition and optical properties of growing surfaces. In a nutshell, the device engineer can control and produce the state of the surface including the composition, crystal structure and smoothness and subsequently, the quality of the material very precisely, and the surface scientist can study, directly, the real-time evolution of surface structure, microstructure and composition. The advantages of the MBE systems over the conventional systems can be summarized as:

- The growth process is controlled to atomic scales of the order of $5\mathring{A}$ due to low growth rates to create smooth and perfect surfaces.
- The low temperature environment, preventing the mixing of multi-layered structures, and the beam nature of sources help to grow heterointerfaces.
- Clean growth environment.
- The flux are controlled precisely by computerized systems. Coupled with low growth rates, the composition of the growing epilayer can be modulated within a monolayer scale.

- Constant $in-situ$ monitoring and control of growth is possible using analytical tools like RHEED.

- Compatibility with other high vacuum thin-film processing methods such as ion implantation.

2.2 Low Temperature MBE growth of GaAs

The substrate temperature is a critical parameter in determining the crystal quality of semiconductor films grown by MBE or other epitaxial methods. The growth of high quality epitaxial $GaAs$ layers with low concentration of deep traps by MBE is usually performed in the temperature range of 550 to 650°C [37]. It is also known that growth at temperatures lower than 500°C lead to a very high concentration of deep traps [42] and low carrier mobilities due to the compensating crystal effect. Detrimental effects like diffusion and segregation occur at this high temperatures when high doping is to be done for certain applications like the base region of hetero- junction bipolar transistor (HBT). Because the rate of solid-state diffusion decreases exponentially with decreasing temperature, growth of $GaAs$ at low substrate temperatures would be advantageous if high-quality films could be obtained. Such growth would be expected to produce more abrupt doping profiles, reduce out-diffusion of impurities from the substrate into active regions and decrease inter-diffusion of atoms at heterojunction interfaces. In 1978, Murotani *et al* [1] first observed the crystallinity and semi-insulating properties of non-stoichiometric Low Temperature grown $GaAs$, even when doped heavily at 400°C. After 10 years, Smith *et al* [3] showed that the material remained crystalline even at 200°C. Later, even at 140°C, $GaAs$ epitaxy was observed [43]. It was also observed that only within a critical thickness, which is a function of amount of excess arsenic incorporated, the material remained single crystalline. The crystal defects formed because Ga and As atoms adsorbed on the

substrate from the vapor phase are incorporated into the growing film before they reach appropriate lattice sites by surface diffusion. The defect concentration can be decreased by increasing the temperature or by decreasing the growth rate [44].

It was shown that back-gating and light sensitivity in metal-semiconductor field-effect transistors (MESFET) could be eliminated by growing a semi-insulating $GaAs$ buffer layer at 200°C and annealing at 600°C. [3] In short channel FETs, the parasitic source to drain current through the buffer-substrate region is minimized due to the semi-insulating property [45]. MESFET with better forward and breakdown voltages has become possible with LT GaAs [46]. It was also shown [47] that if grown on LT GaAs buffer layers, the high electron mobility transistors (HEMT) have the benefit of having the diffusion of impurities from the substrate to the active layers slowed down. Lin *et al* [48] showed the elimination of side-gating in HEMTs but observed out-diffusion of defects from the buffer layer to the active regions, resulting in degradation of the high-frequency performance and minimized the effect by using a multi-substrate temperature procedure during MBE of the buffer regions.

Solomon *et al* [49] demonstrated the reduction in back-gating in GaAs semiconductor-insulator-semiconductor FETs (SISFETs). Subramanian *et al* [50] have shown that the semi-insulating properties can be used for isolation of optical devices by using GaAs:As for isolation between tandem solar cells. It can also be used as a current-blocking layer in diode lasers [51]. LT GaAs has applications as high-speed photo-conductor because of its subpicosecond carrier lifetimes and high mobilities. Rahman *et al* [52] have used LT GaAs:As as the photoconducting switch to launch freely propagating electromagnetic pulses.

2.2.1 Point defects in LT GaAs growth

The incorporation of excess *As* in the form of point defects, such as arsenic antisites, arsenic interstitials and gallium vacancies, is critical to understand the interesting properties like short carrier lifetimes of LT GaAs. The LT GaAs grown at about 200°C contains up to 1.5% excess *As*. This excess arsenic dilates the lattice thus straining it [5]. But the structural quality of the epilayer is good [53]. When annealed at 600°C for 10 to 30 minutes, the lattice mismatch caused by the excess *As* reduces [5]. This strain relaxation is accompanied by conglomeration of the excess arsenic [2]. The amount of excess *As* can be controlled with the substrate temperature during MBE. The lower the substrate temperature, the greater is the amount of excess arsenic that is incorporated [54]. Melloch *et al* [55] cycled the substrate temperature to 600°C after a growth of 2μm of material and then brought back to the growth temperature of 250°C thereby, relaxing the strain before the critical thickness is reached and hence showed that LT GaAs with any arbitrary thickness can be grown. The arsenic antisite was observed first in LT GaAs as point defect. Results of electron paramagnetic resonance (EPR) [5] and absorption experiments [56] show the presence of *As* antisites, although these experiments cannot determine if they are isolated or if they occur primarily in complexes involving other point defects. The antisite concentration varies for different samples and different growth conditions but total measured concentration accounts for most of the deviation from stoichiometry in LT GaAs. The concentration of charged As_{Ga}^{+} measured by EPR was found to be in the order of 1 to 5 x 10^{18}cm^{-3} and neutral antisites, As_{Ga}^{0} measured by absorption measurements was about 1 x 10^{20}cm^{-3} for the layers grown at 200°C. As the point defect concentration is more, the material exhibits hopping conductivity with resistivities as low as 10Ωcm. Upon annealing the resistivity increases dramatically.

The part of excess *As* which is not observed as antisites exist as *Ga* vacancies

as evidenced by slow positron annihilation experiments [57] or as arsenic interstitials as evidenced by both rapid diffusion and ion channeling experiments [58]. However, these measurements involve many approximations. Initial theoretical studies [59] on As_i considered only tetrahedral configurations and predicted the concentration to be much less than antisites and vacancies in As-rich $GaAs$. In addition, As_i were found to be donors and hence was suggested that the dominant acceptors in LT GaAs must be Ga vacancies. Later theoretical investigations on As_i showed that the As_i are not tetrahedral, but split-interstitial configurations [60]. Though it was presumed initially that the concentration of As^{+}_{Ga} is equal to concentration of ionized acceptors, the ionized Ga vacancy, later it was proved that the Ga vacancy is a triple acceptor, V^{3-}_{Ga}, by comparing the concentration of As^{+}_{Ga} measured by magnetic dichroism of absorption (MCDA) and V_{Ga} measured by slow positron annihilation [9].

Annealed LT GaAs has its electrical properties dependent on point defects and arsenic precipitates. The defect model [61] correlates the decrease in hopping conductivity to the precipitation of excess As, but, the model assumes that the compensation is provided by residual arsenic antisites and not arsenic precipitates. The model proposed a depletion region around As precipitate and the As precipitates are assumed as an embedded Schottky contact. The material properties are controlled by the defects or the Schottky barriers depending on the relative composition of the defects, which in turn, depends on the anneal temperature which when increased to 600°C will transform the material whose properties are dominated by arsenic precipitates. Ibbetson *et al* [62] reported that the room temperature conductivity of the material annealed at 600°C for 30 seconds was due to hopping conductivity and for higher-temperature anneals, it was due to a thermally assisted tunneling process caused by arsenic precipitates.

Liu *et al* [63] studied the structural properties of the LT GaAs by a high-resolution

X-ray diffractometer and measured the concentration of As^0_{Ga} and As^+_{Ga} by optical measurements such as near infrared absorption (NIRA) and magnetic circular dichroism (MCDA) and suggest that the dominant defects are As_{Ga} and V_{Ga} and that the amount of As_i is negligible. Since only the ion channeling experiments supported the the presence of As_i as a direct result [64] and as it is believed that the As precipitation upon annealing is attributed to As_i. Additionally, the formation energy of As_i is several eVs higher than that of As_{Ga} and V_{Ga}, the presence of As_i in LT GaAs is very unlikely. Further, the lattice expansion linearly correlates with the concentration of As_{Ga}.

Lagadas *et al* [65] observed the presence of As precipitates by transmission electron microscopy (TEM) in the material annealed at 600°C and the dependence of excess As incorporation on the growth temperature and BEP. Their theoretical model based on mass balance equation showed that the incorporation of excess As on the surface depends on the growth temperature, BEP and the evaporation of arsenic molecules from the physisorbed state considered in the model.

Luysberg *et al* [36] studied the growth of LT GaAs by NIRA, MCDA and slow positron annihilation under various growth conditions. They showed that at a fixed temperature, the lattice mismatch increased linearly with BEP upto a critical BEP and then saturated. The saturation value is higher for lower temperatures. They also studied that the concentration of neutral and charged antisites at different growth parameters. At a fixed temperature, the concentration of neutral and charged antisites increased with the increase in BEP upto a critical value of BEP and then saturated. At a higher temperature, the defect concentrations decreased as indicated by the previous results. The concentration of As^0_{Ga} was always an order of magnitude higher than that of As^+_{Ga}. Further studies showed that the ultra-fast electron trapping time measured in LT GaAs is related to the presence of As^+_{Ga} [9]. They studied the material

by doping highly with p-type Be to increase the concentration of As_{Ga}^{+} to improve on the trapping time characteristics.

2.3 InGaAs MBE Growth Studies

2.3.1 Segregation Studies

The advantages of gallium arsenide over silicon is the ability of $GaAs$ to allow the introduction of compound semiconductors such as $GaAl$As, $GaInAs$ on $GaAs$ substrates with unique properties that can not perform by silicon. There are several articles addressing the issue of surface segregation, desorption and grading of heterointerfaces [19-35]. In this section, a brief summary of the salient features is presented.

In the desorption mass spectrometry experiments reported [19], a UTI mass spectrometer was used for measuring the desorbing indium signal and a thermocouple is in direct contact to the back of the substrate holder to measure substrate temperature. In desorption spectra as a function of substrate temperature was obtained during growth of $In_{0.21}Ga_{0.79}As$ on $GaAs$ MBE for different pressure of As_4 and As_2 at V/III ratios 17:1 and 36:1. They observed that for low pressures, there are two desorption mechanisms operating whereas for high pressures, it is only one.The activation energy for desorption of 1.3 eV obtained from the data was found to be independent of arsenic species and pressures. They also confirmed that using higher pressures and the use of arsenic dimers improves In incorporation. Additionally, their data indicated that the In surface population controls the In incorporation.

Muraki *et al* [27] found that there is a strong dependence of In surface segregation on the growth conditions. They computed λ from secondary ion mass spectroscopy (SIMS) using the relation R=exp(-d/lanmda) where d is half the lattice constant of

$GaAs$(2.83 Å) where R is the segregation coefficient which can be obtained from

$$x_n = x_0(1 - R^n) \tag{2.1}$$

where n is the number of the layer and x_n and x_0 are the In compositions in the first and the n^{th} layers, respectively. For an increase of growth temperature from 370 C to 520 C, the segregation length λ, was observed to increase from 0.8 to 2.9 nm.

Evans *et al* [24] investigated the evolution of the surface chemistry during the MBE growth of $GaAs/In_{0.22}Ga_{0.78}As/GaAs$ using temperature programmed desorption (TAD) measurements. A low binding peak at 1.5 eV was identified with the surface segregated In. Integration of the TPD provides a quantitative measure of the surface In population. It was found that both $GaAs$ on $InGaAs$ and $InGaAs$ on $GaAs$ are graded in In composition. Predepostion of a thin In layer before the start of the $InGaAs$ growth and flash-off (evaporate by raising temperature temporarily) the surface In before the growth of $GaAs$ aids in achieving a more abrupt composition profile.

Woodbridge *et al* [28] has found that indium segregates to the surface during growth above 550 C and a constant surface concentration forms at low indium flux. Up to two monolayers of indium segregates onto the surface during the growth of 200 $\AA$ of $In_{0.25}Ga_{0.75}As$ at 560 C. further studies are reported for indium segregation at higher substrate temperature including the effects of indium flux and arsenic to group III (V/III) (20:1, 30:1) ratios on the these processes.

The segregation to the surface of third-column atoms in ternary arsenides ($GaAlAs$, $InAlAs$, $InGaAs$) grown by molecular beam epitaxy has been investigated by Hazay *et al* [35] The tendency of third-column atoms to surface segregation in ternary alloys was observed to follow the relation $In > Ga > Al$. The surface segregation of third-column atoms used ternary alloys ($Ga_{0.7}Al_{0.3}As$, $In_{0.52}Al_{0.48}As$, $In_{0.53}Ga_{0.47}As$, $In_{0.2}Ga_{0.8}As$) was studied by *in situ* Auger electron spectroscopy (AES) and X-ray

photo-emission spectroscopy (XPS). The peak of intensities due to the various alloys were considered. The reduced segregation rate, R, relevant to elements A and B in $A_xB_{1-x}As$ is assumed as following:

$$R_A = X_b + (X_s - X_b)[1 - exp(-\frac{a^*}{L_A}] \tag{2.2}$$

$$R_B = 1 - X_b + (X_b - X_s)[1 - exp(-\frac{a^*}{L_B}] \tag{2.3}$$

where a^* is half the lattice constant, X_s and X_b are the surface and bulk compositions of the A element, respectively, and L_A abd L_B are the segregation lengths for elements A and B, respectively. It was suggested that segregation was at origin of variations in the compositional inhomogeneities found at the interfaces such as $GaAs - InGaAs$ normal and inverted interfaces.

One other effect of In surface segregation during the growth of $InGaAs$ on $GaAs$ by MBE is the indium atoms segregation at a ratio of more than 0.8 under the conventional growth conditions for $InGaAs$. The transition form two-dimensional to three-dimensional growth occurs when the amount of indium reaches around 1.7 monolayers with nominal alloy composition greater than 0.25 [34].

2.3.2 Desorption Studies

The desorption of group III elements during MBE of III-V semiconductors is of great importance in the control of the thickness and composition of structures grown. There are two main techniques used in the study of this phenomenon. One is to observe the temperature dependence of the growth rate and infer the desorption rate [19,21,24,25]. The other is to measure the desorption flux directly using modulated beam mass spectroscopy [MBMS]. Measurement of the growth rate can be achieved in-situ by the reflection high energy electron diffraction (RHEED) intensity oscillation technique or ex-situ by layer thickness measurements.

Zhang *et al* [21] have reported two distinct temperature dependences of indium desorption from InAs. One is shown to be independent of surface indium adatom population, the other is shown to be dependent on indium adatom population. They are the rate limiting processes at different temperature regions and are independent of one another. The desorption rate under Langmuir free evaporation can be measured directly by using RHEED, but this method is not as precise as MBMS for growing surfaces. The MBMS technique can be applied to either Langmuir evaporation or growing surfaces. For Ga desorption studies, $GaAs$ or $InAs$ was grown for 10 min at 580'C and 430'C, respectively. The substrate temperatures was in the desired range of 560 C to 630 C. In and Ga molecular beam fluxes were given including As_2 and As_4 were measured using RHEED intensity oscillation and maintained constant. The logarithmic desorption rate Ga from $GaAs$ surfaces is plotted against inverse substrate temperature. Their results have shown that there is a small difference in the desorption rate between the two cases Langmuir evaporation and growing conditions and the activation energy for desorption is approximately 4.0 eV for As_2. For the case of As_4, it was 2.9 and 3.6 eV, for Langmuir free evaporation and evaporation during growth, respectively.

In other study of indium desorption by Mozume *et al* [34], the desorption rate during the molecular beam epitaxy of $InGaAs/GaAs$ growth has been investigated by RHEED intensity oscillations.The InAs mole-fraction was varied from 0.07 to 0.25. Ga, In and As fluxes were monitored by the ion gauge at the substrate position. The V/III flux ratios were varied from 8 to 20. The growth rate was about 0.5 μm/h for $GaAs$. The indium desorption activation energy resulting from the temperature dependence of $InAs$ growth rate agrees with the enthalpy of $InAs$ decomposition.

2.4 RHEED

RHEED is the routinely used surface analytical tool to study the dynamics of *in situ* film growth. In RHEED, a high energy beam of electrons in the range of 5-40 kV is directed towards the surface at a grazing angle of about 1^o to 3^o. This is ideal for MBE where the molecular beams impinge on the surface at near-normal incidence. The glancing angle reflection geometry exploits the strong forward scattering of high-energy electrons by atoms and leads to a very high surface sensitivity. The de Broglie wavelength of these electrons is in the range of 0.18-0.06 $\AA$. The energy component perpendicular to the surface is around 100 eV. Hence, the penetration of the beam into the surface is low, restricted to the top few atomic layers. The geometrical aspects of the electron diffraction pattern can be explained based on limited penetration and hence by kinematic theory of electron diffraction. The smooth surface with periodic arrangement of atoms acts as a two-dimensional grating and diffracts the incident electron beam. The diffraction pattern is recoded by the fluorescent screen placed diametrically opposite the electron gun.

A plane monochromatic wave incident upon a specimen gives rise to an elementary secondary wave in each element of its volume. The incident wave reaches different points of the volume in different phases and consequently the secondary waves arising from these points also have different phases. The amplitude of scattering in its mathematical form represents a Fourier integral. The required fundamentals of the theory of scattering and of structure analysis can be obtained from the theory of Fourier integrals and from Fourier series. Thus, the relationship between the reciprocal lattice and the planes of the direct lattice for a two dimensional non-orthogonal cell can be obtained. Using Bragg's Law and the reciprocal lattice concept, the atom periodicities in the solid surface region can be found by measuring the diffraction spot spacings. The relation between the interplanar distance in the crystal d and the

observed diffraction pattern on the fluorescent screen is given by [66]:

$$d = \frac{4\lambda L}{D} \tag{2.4}$$

where L is the distance between the substrate and the screen and D is the spacing on the screen between beams.

The diffraction is not always a true reflection. If the surface is rough, the pattern is caused by transmission-reflection diffraction and exhibits spotty features. If the surface is smooth, the features look streaky because of the true reflection diffraction [67]. The high specular intensity caused initially is due to the smoothness of the surface.

2.4.1 RHEED Oscillations during MBE

The oscillations of the specular beam intensity as a function of time during MBE was first observed in 1981 [68]. The RHEED oscillations are used to determine growth rates, mole fractions, and quantum well thicknesses. When the growth of the layer is initialized, nucleation occurs and the specular intensity decreases due to destructive interference of the reflected electron beam from the rough surfaces. As the layer fills up, the surface becomes smoother and hence the constructive interference increases which in turn, results in higher specular beam intensity. Layer-by-layer epitaxy with alternate roughening and smoothening of the surface, indicative of significant surface migration, causes RHEED intensity oscillations (ROs) to occur with a period equal to a monolayer deposition time [10,11]. If the migration is limited due to growth conditions, the surface will be rougher which results in decreased amplitude of ROs. The surface migration length changes the period measured due to the competition between step-flow growth and 2D nucleation, for growth on vicinal surfaces, under constant fluxes. Petrich *et al* [69] found differences between measured period and growth rate when *Ga* diffusion length was comparable with the terrace length while

calculating expected intensity oscillations during growth on a vicinal surface. Resh *et al* [70] found that the differences are much more when they added nucleation to this model.

Numerical simulations were carried out by Shitara *et al* [71] and showed that the intensity oscillation period varied with growth temperature. Sudijono *et al* [72] reported that the ROs disappear above the temperature at which the growth proceeds by step flow, in which the step density on the growing surface remains constant. Dabiran *et al* [73] reported that at a constant *Ga* flux, the period of RHEED oscillations during *GaAs* growth on an As-stabilized (111) B surface depends on *As* flux. Since migration length of *Ga* decreases with decrease in temperature, it was believed that the growth of the crystal is not possible at low temperatures and hence no ROs were expected at low temperatures. Ibbetson *et al* [14] reported the occurrence of ROs at low temperatures with near stoichiometric flux ratios and suggested that the growth is a layer-by-layer process. They proposed that the process is very sensitive to BEP and that the ROs were observed only under stoichiometric conditions with no excess *As* present. Recently, Shen *et al* [18] reported the observance of ROs, over a wide range of BEPs from 12 to 100 at a fixed temperature of 300°C and over temperatures ranging from 150 to 750°C at a fixed BEP of 40, suggesting that the stoichiometric condition is not mandatory for the occurrence of ROs. The theoretical model of Venkatasubramanian *et al* [17] explained the cause of the ROs based on a physisorbed state of *As* lying above the growing surface and loosely connected to the surface dictating the incorporation of *As*. They reported that the coverage of this PA layer varied from 0.24 to 0.72.

2.5 Theoretical modeling of MBE growth

Realistic theoretical models of crystal growth by MBE have been developed. Using continuous space models, the assumption of the Hamiltonian is sufficient to describe the physical behavior of the system and are more closer to reality. Conventionally, by discrete models, thermodynamical theories were used to describe processes such as condensation, re-evaporation and incorporation of dislocations. Ab-initio calculations have been made possible with latest computer technologies with realistic interaction potentials. With these microscopic models, the position of the atoms in the growth processes can be simulated in the given conditions and the growth can be better understood. Various theoretical models developed are based on Monte Carlo simulations [74-88], Molecular dynamics [79-81], the stochastic models [10,82-86] and the kinetic rate equation models [17,87].

The widely used technique for modeling MBE processes is Monte Carlo simulation which is done by random sampling [74-88]. The algorithm is based on thermodynamic equilibrium. The properties of the growth system under equilibrium are calculated from its distribution function in the phase space. The size of the growing crystal is taken to be n x n lattice with upto 10 layers building up. The surface processes like incorporation of atoms on the surface, migration and back evaporation from the surface are considered. The system is disturbed by the insertion of a new particle which is incorporated into the growing crystal and then brought to equilibrium until the change in the potential energy by more MC steps is negligible. By repeating this procedure several times, dynamic processes are simulated. Migration and back evaporation processes are taken to be of Arrhenius type with activation energies and frequency factors. MC models represent the substrate and kinetics simply and are easy to implement but consumes more computational time.

Molecular dynamics simulations [79-81] can solve the equation of motion of the

molecules based on Newton's second law of motion and the potential energy functions of semiconductors like Leonard-Jones [79] and Stillinger and Weber potential functions [89]. The surface kinetics of the atoms in picosecond scales are simulated using the classical dynamical equations of motion. The solution of the coupled equations of motion for any particle of the system in MD restricts the number of particles and also the range of real time simulation because of limitations in CPU time. The specific advantage of MD simulations is that the surface kinetics can be studied to get atomistic details.

Rate equation model [17,87] calculates the time evolution of the change of concentration in each epilayer caused by the surface kinetic processes such as incorporation, migration and evaporation occurring on the surface during growth [87]. The model involves solving simultaneous non-linear differential equations and hence computationally less intensive but does not provide microscopic details of the atoms.

Venkatasubramanian [82] developed a stochastic model for the MBE growth kinetic studies of compound semiconductors based on the work of Saito *et al* [85]. The model developed at first for diamond cubic lattice and later for the two-sublattice zinc blende structure was based on the master equation approach and modified solid-solid restriction whereby the atom is not absorbed exactly on top of another atom but in a vacant site whose projection falls in between a pair of nearest neighbor atoms. The time evolution of the epilayer is described by the rate of change of a complete set of macrovariables such as coverage of atoms in a layer, atom-atom pair concentration etc. The model was employed to study the surface roughening kinetics in *Ge* [86]. The kinetics of the LT GaAs were studied using the modified model [17] which in addition to the surface processes like incorporation, evaporation and migration, included the kinetics of the physisorbed layer of *As*, loosely bound to the surface of the growing crystal by Van der Waal type binding. The thermally activated surface processes are

considered rate limiting to dictate the growth of the film. The presence of the PA layer affects the *in-situ* monitoring of the growth by RHEED. The RHEED beam will interact with both the PA layer and the crystalline surface and the amplitude of the ROs will vary with the coverage of physisorbed arsenic. The model was used to study the RHEED intensity dynamics over a wide range of growth conditions. The model considered the factor that As stayed in the physisorbed state with lifetimes in the range of 10^{-3} to 10^{-5} s and incorporated only when an appropriate configuration of Ga atoms formed on the surface. The stochastic model is simple, not limited by the crystal size and can be employed to study the doping kinetics in the crystals.

The modified stochastic model [10] developed by Muthuvenkatraman *et al* considers the growth kinetics of the physisorbed arsenic (PA) layer with the inclusion of the chemisorption of As into the surface antisites from the physisorbed state and the evaporation from these surface antisites. The antisite incorporation from the PA layer and the evaporation of the antisites are taken to be temperature dependent and fitted to Arrhenius form of equations with incorporation lifetime τ_{in} and evaporation lifetime τ_{ev} factors and activation energies for incorporation and evaporation. The model was employed to study the antisite incorporation in the growth of $LT-GaAs$. The dependences of As_{Ga} and the resultant lattice mismatch on various growth parameters like arsenic flux, temperature and growth rate were explained by this model.

CHAPTER 3

THE RATE EQUATION MODEL FOR GROWTH OF III-V COMPOUNDS

3.1 The Kinetic Rate Equation Model

MBE growth involves several surface kinetic processes such as the adsorption and the evaporation, and the surface diffusion processes such as the intralayer diffusion and the interlayer diffusion. The rate of adsorption depends on the flux rate, J, and the availability of proper sites on the surface for adsorption. The evaporation, segregation and diffusion processes are assumed to be thermally activated and are modeled as Arrhenius type with frequency factor and activation energy given by:

$$R = R_0 e^{\frac{-E_{act}}{k_B T}} \tag{3.1}$$

where R_0 is the frequency prefactor, E_{act} is the activation energy, k_B is the Boltzmann constant and T is the temperature in Kelvin. The atom interactions are assumed pairwise and only up to second nearest neighbor interactions are considered. The activation energy for the segregation process, i.e., from the crystal to the physisorbed state, is assumed to be smaller than that for the evaporation process, but larger than that of the surface diffusion process.

The time evolution of the growing epilayer is described through the change of macrovariables resulting from the surface processes. The macrovariables of growth are normalized with respect to the maximum number of possible atoms in the layer. The macrovariables considered are the layer coverage of Ga, As and As_{Ga} in the layers given as:

$C_{Ga}(2n)$: layer coverage of Ga in the 2nthlayer

$$C_{As}(2n+1) \;:\; \text{layer coverage of } As \text{ in the 2n+1}^{th}\text{layer}$$
$$C_{As_{Ga}}(2n) \;:\; \text{layer coverage of antisite } As \text{ in the 2n}^{th}\text{layer} \qquad (3.2)$$

where n is the layer index, with the regular Ga and antisite As belonging to even numbered layers, and the regular As belonging to the odd numbered layers. The layer coverage of atoms is 1, when the layer is completely full and 0, when the layer is completely empty.

Low temperature MBE growth of $GaAs$ will involve additional physics related to possible presence of physisorbed molecules of incoming beams [89,90]. Typically these molecules form a weakly bound precursor state with Van der Waal type binding. This layer of material undergoes two dynamic processes, chemisorption into regular and antisites and desorption [10,85,89,90]. A schematic diagram illustrating the surface dynamic processes of the PA layer and antisite As is shown in Figure 4.1. The processes are thermally activated processes and the time constants for these processes which are inverse of the rate processes are described in the Arrhenius rate form as:

$$\tau_{in} = \tau_{0,in} e^{\frac{E_{in}}{kT}} \qquad (3.3)$$
$$\tau_{ev} = \tau_{0,ev} e^{\frac{E_{ev}}{kT}} \qquad (3.4)$$

where $\tau_{0,in}$ and $\tau_{0,ev}$ are time factor constants, E_{in} and E_{ev} refer to activation energy for incorporation and evaporation of antisites, respectively, k is the Boltzmann constant and T is the temperature in K.

The time evolution of the layer coverage of the PA layer, $\frac{dC_{Phy,As}}{dt}$, is given by:

$$\frac{dC_{Phy,As}}{dt} = \left(J_{As} - \frac{dC_{As}}{dt}\right) - \frac{C_{Phy,As}}{\tau_{ev}^{Phy,As}} - \frac{C_{Phy,As} f_{As}}{\tau_{in,re}^{Phy,As}} - \frac{C_{Phy,As} f_{Ga}}{\tau_{in,an}^{Phy,As}} \qquad (3.5)$$

where $C_{Phy,As}$ is the PA layer coverage and is equal to 1, when the layer is completely full and is zero, when the layer is completely empty. J_{As} is the molecular flux of As coming into the PA state and its units here are in atom/sec. The units of flux is usually

in atoms/cm^2.sec. and it can be converted to atom/site.sec which is simply written as atom/sec. The conversion is performed using the effective area per crystalline site which in case of $GaAs$, with lattice constant a=5.6533$\mathring{A}$, is given by a^2/2 and is equal to 15.97$\mathring{A}^2$ in the (100) growth direction. $\frac{dC_{Phy,As}}{dt}$ is the rate of incorporation of As into the epilayer and C_{As} is the total concentration of As in all the crystalline layers. Typically, it is equal to the growth rate or the Ga flux rate, J_{Ga}. In the above equation, the first term denotes the increase in PA coverage due to arrival of As flux into the PA layer. The next three terms denote the net loss of PA layer coverage due to evaporation, chemisorption in to regular As site and As_{Ga} incorporation in to Ga layer, respectively. f_{Ga} and f_{As} represent the fraction of the available surface Ga sites and are time and temperature dependent. τ with respective suffixes represent the corresponding time constants.

The time evolution of the growing epilayer is described through the change of macrovariables resulting from the surface processes. The macrovariables of growth are normalized with respect to the maximum number of possible atoms in the layer. The macrovariables considered are the layer coverage of Ga, As and As_{Ga} in the layers given as:

$$\begin{aligned} C_{Ga}(2n) &: \text{layer coverage of } Ga \text{ in the } 2n^{th}\text{layer} \\ C_{As}(2n+1) &: \text{layer coverage of } As \text{ in the } 2n+1^{th}\text{layer} \\ C_{As_{Ga}}(2n) &: \text{layer coverage of antisite } As \text{ in the } 2n^{th}\text{layer} \end{aligned} \tag{3.6}$$

where n is the layer index, with the regular Ga and antisite As belonging to even numbered layers, and the regular As belonging to the odd numbered layers. The layer coverage of atoms is 1, when the layer is completely full and 0, when the layer is completely empty. The time evolution of the layer coverage of Ga in the $2n^{th}$ layer due to the various surface processes is given by:

$$\frac{dC_{Ga}(2n)}{dt} = \left([C_{As}(2n-1) - C(2n)]\, J_{Ga}\right)(A1) + [C_{As}(2n-1) - C(2n)]$$

$$
\begin{aligned}
\times \quad & \left(R_0 e^{\frac{E_d(2n+2)}{kT}} \left(\frac{C_{Ga}(2n+2)}{C(2n+2)} \right) [C(2n+2) - C_{As}(2n+3)] \right. \\
+ \quad & \left. R_0 e^{\frac{E_d(2n-2)}{kT}} \left(\frac{C_{Ga}(2n-2)}{C(2n-2)} \right) [C(2n-2) - C_{As}(2n-1)] \right) (B1) \\
- \quad & R_0 e^{\frac{E_d(2n)}{kT}} \left(\frac{C_{Ga}(2n)}{C(2n)} \right) [C(2n) - C_{As}(2n+1)] \\
\times \quad & ([C_{As}(2n+1) - C(2n+2)] + [C_{As}(2n-3) - C(2n-2)]) (C1) \\
- \quad & R_0 e^{\frac{E_e(2n)}{kT}} \left(\frac{C_{Ga}(2n)}{C(2n)} \right) [C(2n) - C_{As}(2n+1)] (D1) \qquad (3.7)
\end{aligned}
$$

where the term A1 denotes the increase in $C_{Ga}(2n)$, due to adsorption of Ga from the incoming molecular beam. The rate of adsorption is the product of the available sites for Ga incorporation on the surface, $[C_{As}(2n-1) - C(2n)]$, and the flux of Ga, J_{Ga}. The sticking coefficient of Ga is taken as unity. The term B1 describes the increase in $C_{Ga}(2n)$ due to migration into the $2n^{th}$ layer from adjacent Ga layers indexed (2n+2) and (2n-2) and fraction of available sites for Ga in the $2n^{th}$ layer, $[C(2n-2) - C_{As}(2n-1)]$. The rate of migration is described by Arrhenius type rate equations with frequency factor, R_0 and activation energy, E_d. The cation sublattice contains two possible elements, Ga and antisite, As_{Ga}. Thus,

$$C(2n+2) = C_{Ga}(2n+2) + C_{As_{Ga}}(2n+2)$$

Therefore, of the fraction of the $(2n+2)^{th}$ layer exposed, only a fraction of it is Ga portion. Thus, the fraction $\frac{C_{Ga}(2n+2)}{C(2n+2)}$ is used to make sure that only the Ga portion is considered for migration. Similar arguments hold for the $(2n-2)^{th}$ layer also. The activation energy for a particular layer is a function of layer coverage of that layer, the activation energies of isolated atoms, $E_{d,iso}$, and the second neighbor atom-atom pair interaction energy, $E_{Ga,Ga}$, with a factor of four as there are four possible neighboring atoms present. In the mathematical form, the activation energy for diffusion for the $2n+2^{th}$ Ga layer is given as:

$$E_d(2n-2) = E_{d,iso} + 4E_{GaGa}C_{Ga}(2n-2)$$

Thus $E_d(2n)$ is equal to $E_{d,iso}$ when the coverage is very small, and this is the correct value since there will be no inplane nearest neighbors, and is equal to $E_{d,iso}+4E_{GaGa}$ when the layer is full and is also the correct value in this limit since there will be 4 inplane nearest neighbor atoms. The term C1 denotes the decrease in $C_{Ga}(2n)$ due to migration out of the $2n^{th}$ layer to the adjacent layers, (2n+1) and (2n-3). The description of the rate of this process is similar to term B1, with $E_d(2n)$ being the activation energy for migration from $2n^{th}$ layer, $[C_{As}(2n+1)-C(2n+2)]$ and $[C_{As}(2n-3)-C(2n-2)]$ being the fractions available for Ga atoms to migrate in the adjacent layers (2n+1) and (2n-3) respectively and $[C_{As}(2n)-C(2n+1)]$ being the fraction of Ga atoms in the $2n^{th}$ layer. $\frac{C_{Ga}}{C}$ is the fraction of the $2n^{th}$ layer to which the rate constant is applied. The term D1 describes the evaporation of Ga atoms from the $2n^{th}$ layer resulting in the decrease in $C_{Ga}(2n)$ with activation energy for evaporation, $E_e(2n)$, fraction of the $2n^{th}$ layer exposed, $[C_{As}(2n)-C(2n+1)]$. Note that only the Ga portion of the exposed layer is considered by using the fraction $\frac{C_{Ga}(2n)}{C(2n)}$. The description of the activation energy for evaporation, E_e is similar to that of E_d and is given as:

$$E_e(2n) = E_{e,iso}+4E_{GaGa}C_{Ga}(2n)$$

with $E_{e,iso}$ is the evaporation energy for the isolated atom.

The time evolution of the layer coverage of As_{Ga} in the $2n^{th}$ layer is given as:

$$\begin{aligned}
\frac{dC_{As_{Ga}}(2n)}{dt} &= \left([C_{As}(2n-1)-C(2n)]\,J_{Ga}\right)(A2)+[C_{As}(2n-1)-C(2n)] \\
&\times \left(R_0 e^{\frac{E_d(2n+2)}{kT}}\left(\frac{C_{As_{Ga}}(2n+2)}{C(2n+2)}\right)[C(2n+2)-C_{As}(2n+3)]\right. \\
&+ \left. R_0 e^{\frac{E_d(2n-2)}{kT}}\left(\frac{C_{As_{Ga}}(2n-2)}{C(2n-2)}\right)[C(2n-2)-C_{As}(2n-1)]\right)(B2) \\
&- R_0 e^{\frac{E_d(2n)}{kT}}\left(\frac{C_{As_{Ga}}(2n)}{C(2n)}\right)[C(2n)-C_{As}(2n+1)] \\
&\times \left([C_{As}(2n+1)-C(2n+2)]+[C_{As}(2n-3)-C(2n-2)]\right)(C2)
\end{aligned}$$

$$- \quad R_0 e^{\frac{E_e(2n)}{kT}} \left(\frac{C_{As_{Ga}}(2n)}{C(2n)} \right) [C(2n) - C_{As}(2n+1)] \, (D2) \tag{3.8}$$

Note that Eqn. 3.8 is similar to 3.7 except for the substitution of Ga with As_{Ga}. The activation energies $E_{d,As_{Ga}}$ and $E_{d,As_{Ga}}$ are given by:

$$\begin{aligned} E_{d,As_{Ga}} &= E_{d,As_{Ga},iso} + 4E_{Ga.As_{Ga}} C_{Ga} \\ E_{e,As_{Ga}} &= E_{e,As_{Ga},iso} + 4E_{Ga.As_{Ga}} C_{Ga} \end{aligned}$$

The terms A2, B2, C2 and D2 are similar to that of A1, B1, C1 and D1 in description except for the substitution of Ga with As_{Ga}.

The time evolution of the layer coverage of As in the 2n+1th layer, $C_{As}(2n+1)$, is written as:

$$\begin{aligned} \frac{dC_{As}(2n+1)}{dt} &= ([C(2n) - C(2n+1)] \, J_{As}) \, (A3) + [C(2n) - C(2n+1)] \\ &\times \left(R_0 e^{\frac{E_d(2n+3)}{kT}} \left(\frac{C_{As}(2n+3)}{C(2n+3)} \right) [C(2n+3) - C(2n+4)] \right. \\ &+ \left. R_0 e^{\frac{E_d(2n-1)}{kT}} \left(\frac{C_{As}(2n-1)}{C(2n-1)} \right) [C(2n-1) - C(2n)] \right) (B3) \\ &- R_0 e^{\frac{E_d(2n+1)}{kT}} \left(\frac{C_{As}(2n+1)}{C(2n+1)} \right) [C(2n+1) - C(2n+2)] \\ &\times ([C(2n+2) - C_{Ga}(2n+3)] + [C(2n-2) - C(2n-1)]) \, (C3) \\ &- R_0 e^{\frac{E_e(2n+1)}{kT}} \left(\frac{C_{As}(2n+1)}{C(2n+1)} \right) [C(2n+1) - C(2n+2)] \, (D3) \end{aligned} \tag{3.9}$$

All the terms A3, B3, C3 and D3 can be explained similar to those of Eqn. 3.7.

Thus coupled nonlinear first order differential equations, given by Eqns. 3.7, 3.8 and 3.9, are obtained for the time evolution of all the macrovariables for every layer to be simulated and an additional equation for the PA layer, given by Eqn. 3.5, considered on the surface is also included.

3.2 Computational Details

Description of evolution of each bilayer of $GaAs$ requires 3 first order nonlinear differential equations, one describing the time evolution of each of the normalized

macrovariables. In this work simultaneous growth of 80 bilayers and the PA layer are considered requiring a total of 241 (= 80 x 3 + 1) coupled nonlinear first order differential equations. The system of equations were integrated using a Fourth-order Runge Kutta method with time steps of less than 10^{-6} s to get the values of each of the macrovariables as a function of time for a growth time of 20 s. The growths were simulated on the Silicon Graphics supercomputer ORIGIN-2000. The average coverages of Ga, As and As_{Ga} in individual layers at the end of growth are obtained from the solution of the differential equations by considering the coverage of a few layers in the bulk, viz., the layers far from the substrate and the surface. A fraction of layer coverages of the particular species is obtained by this method. This fraction is converted to concentration per cm^3 using the total number of sites/cm^3 in a sublattice, which in the case of $GaAs$ is 2.21 x $10^{22}/cm^3$.

3.3 Conversion of J_{As} to BEP

Experimentally, the As flux is described in terms of BEP for a given Ga flux, whereas our model requires the flux in number of monomer atoms per site per second. The conversion between the two flux definitions is accomplished using the following equation [91]:

$$\frac{J_{As_4}}{J_{Ga}} = \frac{P_{As_4}}{P_{Ga}} \frac{\eta_{Ga}}{\eta_{As_4}} \sqrt{\frac{T_{As_4}}{T_{Ga}} \times \frac{M_{Ga}}{M_{As_4}}} \tag{3.10}$$

where $\frac{P_{As_4}}{P_{Ga}}$ is the BEP, J is the flux and T is the absolute temperature and M is the molecular weight. η is the ionization efficiency for the respective species relative to nitrogen and is given by:

$$\frac{\eta}{\eta_{N_2}} = \left[\left(\frac{0.4Z}{14}\right) + 0.6\right] \tag{3.11}$$

where η_{N_2} is the ionization efficiency of nitrogen and Z is the atomic number. In this Eqn 3.10, the As is assumed a tetramer. The values used for MBE growth of $GaAs$ are: Z_{Ga}=31; Z_{As_4}=4 x 33; T_{As_4}= 1173K; T_{Ga}=573K; M_{Ga}=69.72 and M_{As_4}=4x74.92

to obtain the value of J_{As_4} as 0.2345(BEP)(J_{Ga}) monomer/site.sec. J_{Ga} is in μm/hr. The number of sites per cm^2 in case of (100) $GaAs$ is obtained as: 1μm/hr. = 2.77 $\AA$/sec.; Since one bilayer of $GaAs$ is half of the cubic lattice constant which is equal to 2.82$\AA$, 0.98 atoms/site.sec. arrive a site for a growth rate of 1μm/hr. The equivalent surface area for a (100) site is 6 x 10^{-16}cm^2 and hence, the number of sites per cm^2 is obtained as 6.26 x 10^{14}. Using the conversion factors described in the above paragraph along with Eqn. 4.2, Eqn. 4.1 can be rewritten as:

$$J_{As}(\text{monomer/cm}^2\text{.sec.}) = 4.0 \times 1.46 \times 10^{14} \times \left(\frac{P_{As_4}}{P_{Ga}}(\text{BEP})\right) J_{Ga}(\mu\text{m/hr.}) \quad (3.12)$$

where 4 is used for converting the tetramer to monomer.

CHAPTER 4

RESULTS AND DISCUSSIONS

4.1 Low Temperature GaAs MBE

4.1.1 Neutral and Charged antisite concentrations

The growth direction considered is [100] and the growth rate is 1μm/hr. for antisite calculations. The growth rate of 1μm/hr. is equivalent to 0.983 atoms/sec. As is assumed to be a monomer, cracked from either As_2 or As_4. Both Ga and As are allowed to incorporate on the surface sites even when only one of the surface covalent bonds is satisfied. This is equivalent to relaxing the modified solid on solid (MSOS) restriction of the initial model [82]. Investigations are done over a temperature range from 423°K to 513°K for the calculations of antisite concentrations over a BEP ranging from 9 to 30.

From the solutions of the differential equations, the coverage of Ga, As and As_{Ga}, viz., C_{Ga}, C_{As} and $C_{As_{Ga}}$, in their respective layers of all the 80 bilayers are obtained using the procedure explained in section 3. In the case of even numbered layers, i.e., Ga sublattices, in addition to Ga, As_{Ga}, there are vacancies, V_{Ga}, present. Hence, the coverage of the even numbered layers, $C(2n)$, is obtained as:

$$C(2n) = C_{Ga}(2n) + C_{As_{Ga}}(2n) \tag{4.1}$$

And the coverage of V_{Ga} in the $2n^{th}$ layer is the sum of all Ga sites not occupied by either Ga or As_{Ga} and is obtained as:

$$C_{V_{Ga}} = 1 - C(2n) \tag{4.2}$$

since the maximum coverage possible in a layer is 1. The Ga vacancies, V_{Ga}, which are present as triple acceptors [9], partially compensate As_{Ga}, a part of which is positively charged. Thus, from the charge neutrality equation, the charged antisite As^{+}_{Ga} coverage is equal to three times that of V_{Ga}. Mathematically,

$$3{V_{Ga}}^{3-} = C^{+}_{As_{Ga}} \tag{4.3}$$

So, V^{3-}_{Ga} and hence $C^{+}_{As_{Ga}}$ can be obtained from the simulation results using Eqns. 4.1-4.3. The total antisite coverage in the $2n^{th}$ layer which is obtained as part of the results of simulation is the sum of charged and neutral antisites:

$$C_{As_{Ga}}(2n) = C_{As^{+}_{Ga}}(2n) + C_{As^{0}_{Ga}}(2n) \tag{4.4}$$

Hence, the coverage of neutral antisites $C_{As^{0}_{Ga}}$ can be obtained by subtracting the coverage of charged antisites, from that of the total antisites $C_{As_{Ga}}$. The layer coverages of antisites for several layers far away from the surface and substrate, *i.e.*, bulk, were found to be uniform for all simulations. These coverages were converted to volume concentrations by using the approach discussed at the end of section 3.2.

Charged and neutral antisite As concentration versus BEP obtained from our simulations were fitted to four experimental data points of Luysberg *et al* [8] to fix the model parameters accurately. The fitted model parameters are reported in Table I. Using the fixed model parameters, model predictions for the remaining growth conditions were obtained.

Plots of As^{0}_{Ga} and As^{+}_{Ga} versus BEP for 513°K and 473°K obtained using the model are shown along with the experimental data of *Luysberg et al.*[8] in Figure 4.2. The agreement between the results is good. Both As^{0}_{Ga} and As^{+}_{Ga} concentrations saturate beyond a BEP of 20 for $513^{o}K$ and $473^{o}K$. The explanation for such a behavior can be given based on the consideration of the PA layer of arsenic. For a given temperature, as BEP increases, the As flux in excess of Ga flux increases,

resulting in increase in the PA layer coverage till the coverage reaches its maximum value of unity at a critical BEP [10]. Beyond the critical BEP, any further increase in BEP does not change the PA layer coverage as it has attained its maximum of monolayer coverage. The As^0_{Ga} and As^+_{Ga} concentrations incorporated in the crystal are dictated by two competing mechanisms, incorporation of As from the PA layer and evaporation of As_{Ga} from the crystal. For a given temperature, the saturation of As_{Ga} occurs because the incorporation and evaporation lifetimes and the PA layer coverage are all constant beyond the critical BEP. Hence the incorporation of As^0_{Ga} and As^+_{Ga} directly depends on the PA layer coverage. The saturation of As_{Ga} concentration is lower for higher temperature because of higher evaporation rate of As_{Ga} from the crystal. The decrease in As^+_{Ga} concentration with increase in temperature is also due to the reason that the migration length of Ga is more at a higher temperature which decreases the Ga vacancy concentration and hence decreases the As^+_{Ga} concentration. Both As^+_{Ga} and As^0_{Ga} exhibit the same dependencies on BEP and temperature, but the As^0_{Ga} is consistently one order of magnitude higher than the concentration of As^+_{Ga}.

3-D plots of the concentration of As^0_{Ga} and As^+_{Ga} respectively with respect to the variation of temperature from 423 K to 513K and BEP from 9 to 30 are shown Figures. 4.3 and 4.4. When the temperature is decreased from 513°K the concentrations of both As^0_{Ga} and As^+_{Ga} continue to increase until a particular value and then saturate at all BEP values. This result is in agreement the experimental results [92] in which the lattice mismatch proportional to As^0_{Ga} was measured. In the experimental measurements below 165°C, the layers became polycrystalline and the lattice mismatch could not be determined. As the temperature decreases from 513°k, the evaporation of As^0_{Ga} from the crystal decreases and becomes negligible at lower temperatures. Hence, the As^0_{Ga} concentration increases. At low temperatures, the PA layer cover-

age is more and at a critical temperature reaches the monolayer coverage which makes the antisite concentration saturate.

A plot of the change in the concentration of As^0_{Ga} for various growth rates in the range of 1-1.5 μm/hr. at 473°K and at a fixed BEP of 20 is shown in Figure 4.5. The As^0_{Ga} concentration decreases when the growth rate is increased at all the values of BEP uniformly. When the growth rate is increased, say from 1μm/hr, the number of Ga atoms arriving at the surface increases. There is a competition between the arriving Ga atoms and the antisite As to occupy the surface cationic sites of the growing crystal. When more number of Ga atoms arrive at the surface, the incorporation of excess As in to antisites decreases and hence the As^0_{Ga} concentration decreases. A similar plot for the concentration of As^+_{Ga} with different growth rates at 473°K and at a fixed BEP of 20 is shown in Figure 4.6. The behavior of As^+_{Ga} concentration and explanation are similar to those of As^0_{Ga}.

Since the concentration of As^+_{Ga} was correlated to the short decay times of excess carriers [6], it was suggested that the response times actually correspond to the trapping time of excess electrons, rather than to carrier recombination times. Hence the temporal response of $LT-GaAs$ can be controlled not only by changing the growth temperature but also by introducing acceptor dopants that allow to increase the concentration of As^+_{Ga}. In undoped $LT-GaAs$, the concentration of As^+_{Ga} was determined mainly by V_{Ga}, the native acceptors of the material. However, the undoped $LT-GaAs$ is metastable, *i.e.*, thermal annealing above 400°C causes lattice relaxation due to As out-diffusion and As precipitate formation. It was found [7] that the ionized antisites are thermally more stable than the neutral antisites. Specht *et al* [9] investigated the high p-doping with Be acceptors to achieve high ionization fraction of the antisites. The Be concentrations in the layers were determined by Secondary Ion Mass Spectrometry (SIMS), the concentration of As^0_{Ga} was determined by NIRA,

the concentration of As_{Ga}^{+} by MCDA and that of V_{Ga} by slow positron annihilation. For a Be concentration of 7 x $10^{19}/cm^3$, the lattice mismatch of the sample grown at 200°C, was found to decrease. This is due to the fact that the size of Be atom is smaller than that of As.

The kinetic rate equation model was used to determine the Be doping kinetics of LT GaAs. Though experimental data are available for Be concentrations, the Be flux is not available without which modeling the doping kinetics with the present model is limited. With the data available, the general trend of the decrease in antisite concentration with increase in Be doping was observed with the model but predictions for different growth parameters could not be performed without the Be flux data.

4.1.2 RHEED Oscillations

The growth direction considered is [100] for RHEED intensity calculations. The range of growth conditions investigated in the study are: temperature in the range of 523-773°K and As beam equivalent pressures in the range of 10-40 at a growth rate of 0.7μm/hr. As is assumed to be a monomer, cracked from either As_2 or As_4. The presence of the PA layer on the surface influences the $in-situ$ monitoring of the growth rate and the surface quality by RHEED. In the presence of the PA layer, the incident RHEED electron beam interacts with both the crystalline surface of the growing crystal and the surface of the PA layer. Hence the amplitude of ROs is dictated not only by the step density variation, but also by the physisorbed layer coverage variation with time. The crystalline surface of the $GaAs$ exposed to the RHEED beam changes with time with respect to the periodic variation of the surface coverage of the PA layer even if the step density is constant. A schematic picture of the RHEED beam interactions with the two surfaces is illustrated in Figure 4.7. A 10kV electron beam incident at 1^o gracing incidence is considered. The scattering from the two distinct surfaces, the PA surface and the exposed crystalline surface,

should be considered and are given by:

$$A_1(t) = \sum_{n=1}^{n=\infty} (C(2n-1) - C(2n))\,(1 - C_{Phy}) \exp\left[i.\left((2n-1)\frac{2\pi}{\lambda}d\right)\right] \quad (4.5)$$

$$A_2(t) = \sum_{n=1}^{n=\infty} (C(2n-1) - C(2n))\,(C_{Phy}) \exp\left[i.\left((2n-1)\frac{2\pi}{\lambda}d + d_{Phy}\right)\right] \quad (4.6)$$

where the term A_1 accounts for the scattered wave amplitude from the exposed crystal and A_2 for that from the PA layer. C_{Phy} is the surface coverage of the PA layer. d_{Phy} is the interplanar distance from the PA layer to the underlying crystalline layer. d is the interplanar distance of the $GaAs$ crystal. λ is the wavelength of incident beam. The resultant specular beam intensity I is given by:

$$I(t) = \sum_{n=1}^{n=\infty} |A_1(2n) + A_2(2n)|^2 \quad (4.7)$$

Note that the coverage variables are a function of time and hence $A_1(t)$, $A_2(t)$ and I(t) will also be a function of time.

RHEED intensity versus time can be computed using growth data of concentration versus time into Eqns. 4.5 - 4.7 with an $As - As$ interplanar distance of 2.48 $\mathring{A}$ for physisorbed As layer and a $Ga - As$ interplanar distance of 1.41 $\mathring{A}$. The interplanar distances considered are quite reasonable since in the PA layer, atoms are loosely connected by Van der Waal type bonding and hence the value should be larger than the crystalline $Ga - As$ bond and close to the gaseous dimer bond length.

Plots of ROs versus time at a BEP of 40 with varying temperatures simulated using our model are shown in Figure 4.8. Comparing the results of Fig. 1 of Ref.[18] to Figure 4.8, the qualitative agreement between the results is good. At an As BEP of 40, the ROs are prominent for temperature above 673^{o}K and below 573^{o}K with a temperature window between 573 and 623^{o}K in which ROs disappear. This behavior can be explained as follows. The growing $GaAs$ surface is partially covered by a layer of physisorbed As which is bonded to chemisorbed crystalline As. Thus, the reflected RHEED intensity has two components, one from the exposed $GaAs$ crystalline surface and the other from physisorbed As. For low temperatures, the surface is almost covered by the physisorbed As whose step density oscillates periodically with the

subsurface crystalline $GaAs$ and hence results in ROs. At high temperatures, the physisorbed As evaporates from the surface and exposes the crystalline $GaAs$ which yields ROs due to periodic step-density oscillations. At intermediate temperatures, the surface is partially covered by the physisorbed As resulting in RHEED intensity from crystalline and physisorbed As surfaces. Due to very different interplanar distances between these layers ie., d_{Ga-As}=1.41$\AA$ and d_{As-As}=2.48$\AA$, complete destructive interference of the two reflected from the PA layer and the crystal results at surface coverage of 0.5 of the PA layer. Thus, there are no ROs in the intermediate temperature range of 573^{o}K and 773^{o}K.

A plot of ROs versus time at 573^{o}K with varying BEPs obtained using the model is shown in Figure 4.9. The results agree qualitatively well with that of Fig. 3 of Ref.[17]. The ROs are observed at a BEP above 40 and below 30 and disappear in the intermediate range. This behavior can be explained based on a reasoning similar to the one presented for the temperature behavior. For high BEPs, the surface is almost covered by the PA layer whose step density oscillates periodically with that of the underlying crystal and hence results in ROs. At low BEPs, due to the reduced overpressure of As, more crystalline surface is exposed to the electron beam which yields ROs due to periodic step density oscillations. At intermediate BEPs, due to the partial surface coverage of the PA layer, the RHEED intensity has both the components interacting with each other. When the PA layer coverage is 0.5, both the reflected beams interfere destructively due to their different interplanar distances to result in no ROs.

ROs versus time obtained by simulation using the model at a growth rate of 1.4μm/hr. at 573^{o}K at various BEP ratios is shown in Figure 4.10. The results are compared with those of Figure 4.8 corresponding to a lower growth rate of 0.7μm/hr. with other growth conditions remaining same. It is obvious from the Figure 4.10 that by doubling the growth rate, the number of layers grown is doubled, at any BEP ratio, which can be observed as the number of ROs in the plots. However, the BEP ratio window at which the ROs are suppressed remains the same between 30 and

40. This is due to the reason that the PA layer coverage remains unaffected by the variation of growth rate.

4.2 InGaAs Segregation and Desorption Studies

The kinetic model for $InGaAs$ growth is similar to that of $GaAs$ growth, except that in this case, antisites are not allowed and additionally, In has a tendency to segregate to the physisorbed material layer (PM). Thus, Figure 4.1 describes the surface dynamics pictorially with appropriate deletions and inclusions of the surface processes.

4.2.1 Model Parameter Fitting Procedure

The model involves several parameters such as time constants and activation energies, which are initially unknown. These unknown parameters are established according to the following procedure. Experimental conditions employed by Fournier *et al* [19] were simulated and the model parameters were adjusted systematically until In incorporation coefficient values for substrate temperature 803 and 903°K fitted well with the experimental data for a As_4 BEP of 36. Once the parameters were established, these parameters were used for the rest of the simulations with As_4 and As_2 at growth conditions employed by several independent research groups [19-29]. Detailed descriptions of these parameters and their values are discussed below.

The activation energy for incorporation processes of Ga and As from the PM layer to the crystal surface are assumed to be independent of temperature (i.e., E_{in}^{Ga}=0.0 eV and E_{in}^{As}=1.0 eV). The activation energy for the incorporation of In from the PM layer onto the crystal, E_{in}^{In} is assumed to be linearly dependent on the In coverage in the physisorbed layer and is given by:

$$E_{in}^{In} = 0.5 C_{In,phy} \tag{4.8}$$

where $C_{In,phy}$ is the coverage of In in the PM layer. Similarly the activation energies for the In, Ga and As evaporation process from the PM layer, E_{ev}^{In}, E_{ev}^{Ga} and E_{ev}^{As} are

assumed to be linearly dependent on their own coverage in the physisorbed layer and are given by:

$$\begin{aligned} E_{ev}^{In} &= 0.18 + 0.06 C_{In,phy} \\ E_{ev}^{Ga} &= 0.18 + 0.06 C_{Ga,phy} \\ E_{ev}^{As} &= 0.18 + 0.06 C_{As,phy} \end{aligned}$$

The prefactor of time constants for incorporation and evaporation processes are obtained according to the Arrhenius equation and related to the activation energies which were described earlier.

The evaporation, segregation and diffusion processes in the surface of the epilayer are assumed to be thermally activated and are modeled with the frequency factor, R_0 and activation energy. R_0 is also linearly dependent on the substrate temperature, and is given by:

$$R_0 = 2.08 \times 10^{10} \times T$$

This is based on the phonon frequency obtained using the equi-partition energy principle. The frequency prefactor of diffusion processes are assumed constants. The frequency prefactor of In segregation is considered to be linearly dependent on the substrate temperature, and is given by:

$$R_{0,s} = 1.743 \times 10^{10} \times T$$

The segregation process from the PM layer is allowed only for In. It is noted that $R_{0,s}$ is smaller than the R_0 of evaporation and diffusion. All the model parameters and their dependences on the surface coverage are summarized in Table II.

4.2.2 InGaAs Segregation and Desorption Studies

For this study, the growth conditions of Fournier *et al* [19] were used. The fluxes were: J_{Ga}=0.714 μm/h; J_{In}=0.192 μm/h; J_{As4} and J_{As2} BEP in the range of 17 to

36. The substrate temperature was in the range of 500-700°C. The In incorporation coefficient, which is defined as a ratio of the total In incorporated to the total In deposited, was obtained for various growth temperature for both As_4 and As_2 for a BEP of 36. Plots of In incorporation coefficient versus substrate temperature obtained from simulation are shown in Figure 4.11 along with the experimental results of Fournier *et al* [19]. The agreement is excellent for As_4 and fair for As_2 for entire temperature range. It is noted that there is no difference between the model parameters for As_4 and As_2. The In incorporation decreases with temperature for both As_4 and As_2 due to increased segregation of In to the PM layer and evaporation of In to the vacuum. The In incorporation coefficient is larger for As_2 than As_4 at the same BEP. The primary reason for this is that the actual flux of As monomer/ site.sec. for As_2 is more than that of As_4 given by Eqn. 3.12. Thus, in our model, no difference in reactivity between As_4 and As_2 is considered which makes the model simple to use.

Plots of In incorporation coefficient versus temperature for As_4 BEP of 17 along with the experimental results of Fournier *et al* [19] are shown in Figure 4.12. The agreement between the results in excellent below 570°C. Above 570°C, simulation results are lower than the experimental values but agree well with the values for BEP of 36. The experimental values saturate at 0.2, even though the physical reasons suggest that at 630°C, it should be close to zero, especially since the incorporation coefficient is close to zero for BEP 36.

Plots of In incorporation coefficient versus temperature are shown for various As_4 BEPs in Figure 4.13. As BEP increases, the incorporation coefficient increases due to reduced lifetime for In surface atoms for the evaporation and segregation processes. It is observed that to achieve a high In incorporation a low substrate temperature below 570°C and high BEP of As_4 above 17 are needed.

Desorption parameter of the i^{th} species, D_i, was found as the difference between the arriving atoms and the change in the total atom concentration in the crystal and

the PM layer in a preset short period of time. Mathematically, it can be written as:

$$D_i = J_i(\Delta t - \left[\sum_{\text{all grown layers}} [C_i(2n)(t+\Delta t) - C_i(2n)(t)]\right]) - [C_{i,phy}(t+\Delta t) - C_{i,phy}(t)] \tag{4.9}$$

where Δt was arbitrarily chosen as 0.1 s for the simulation. The In and Ga fluxes were on from 0 to 5 s and at 5 s, the In flux was terminated. Plots of In desorption parameters, D_{In}, (computed using Eqn. 4.9) versus time for a As_4 BEP of 36 is shown in Figure 4.14. These results agree qualitatively well with the experimental results of Ref.[19]. A quantitative comparison can not be made due to the arbitrary nature of the experimental results. The In desorption rate initially increases rapidly and reaches a steady state within 2 seconds. After the In flux is terminated, the In desorption flux decreases exponentially to zero. As expected, the desorption rate is larger for higher temperatures. Additionally, D_{In} shows periodic oscillations in the desorption flux which is related to the periodic exposure of the cation and anion layers due to layer-by-layer evaporation from the crystal. Even though there are noticeable oscillations in the experimental data [19], it is not as periodic as our results.

Indium desorption parameters versus time is shown in Figure 4.15 for 903°K for As_4 BEPs of 36 and 17. The indium desorption for higher BEP are smaller as the effective time allowed for evaporation of In before a As molecule adsorbs on top of it is smaller for higher BEP.

Relative desorption parameter (RDP) is defined as the ratio of steady state desorption parameter $D_{In}(T)$ to $D_{In}(803^oK)$ where 803°K is the lowest temperature in our study. RDP was obtained for several temperatures from Figure 4.14 for a As_4 BEP of 36. A plot of RDP versus substrate temperature is shown that along with the experimental data of Fournier *et al* [19] is shown in Figure 4.16. The agreement between the results is excellent for most of the temperature range. Experimental [19] as simulation plots of RDP versus temperature for a As_4 BEP of 17 shown in Figure 4.16 also shows good agreement.

The MBE growth simulation was also performed for $GaAs$ growth experiments

of Kao *et al* [26]. Simulated gallium desorption parameters, D_{Ga} given by equation similar to Eqn. 4.9 in the presence of As_4 flux is shown in Figure 4.17. The activation energy for desorption was found 2.92 eV from Figure 4.17. This value of 2.92 eV is smaller than that obtained by Kao *et al* [26]. But our value is reasonable, considering the fact that a surface Ga surrounded by four in-plane Ga neighbors will have an activation energy of about 3.5 eV and a Ga is surrounded by by two in-plane Ga atoms will have about 3.1 eV. Our investigations strengthened the previous suggestions in the literature [19] that there are two components to the desorption process, one from the surface riding In and the other from the crystal. The activation energy for these processes for an isolated adatom are 0.18 eV and 2.6 eV, respectively.

Plots of In layer composition versus layer number is shown in Figure 4.18 for various substrate temperature at a BEP of 36. The growth simulation were performed for 10 s at a growth rate of 0.912 ML/s. These results agree fairly well with the experimental results of Ref. [26]. At lower temperatures the In composition uniform over 10 layers for most temperatures. The segregation of In spreads over at least 10 layers which suggests that these will considerable roughness of alloy mixing at heterointerfaces.

Segregation coefficient, R, can be obtained using the data Figure 4.18 and the following equation:

$$logR = \frac{1}{n} log\left(1 - \frac{x_n}{x_o}\right) \tag{4.10}$$

where n is the number of the layer and x_o and x_n are the nominal composition and the composition of the n^{th} layer, respectively. Plots of R versus temperature obtained for several BEPs of As_2 and As_4 is shown along with the experimental data of Kao *et al* [26] for As_4 BEP of 6 in Figure 4.19. Qualitatively, the results are in good agreement. In general, the segregation coefficient, R increases non-linearly with temperature and attains a maximum value of 1.0 at 850^{o}K for a As_4 BEP of 17. The temperature at which the maximum R is attained increases with BEP as segregation rate decreases with BEP.

4.2.3 General Observations and Growth Implications

- The In incorporation to the surface layer decreases in substrate temperature higher than 540°C, more indium atoms incorporate to the the growth surface when the BEP ratio is higher than 20.

- The In segregation rate is large for higher temperatures and low As over-pressure. Thus, to minimize the In segregation, one should adopt lower temperatures and high As over-pressures. But, the temperature should not be set so low that the other thermally activated surface processes such as migration and As molecular adsorption by reaction are suppressed.

- The In desorption for BEP of 36 has a higher rate compare to 17, the actual desorption ratio shows the same behavior in experiment and simulation, it goes up more rapidly by increasing substrate temperature when BEP is higher.

- In desorption has two components, one from the surface riding In layer and the other from the surface of the crystal itself. The former component is smaller than the latter.

- As_2 limits the In segregation rate more As_4 of the same BEP and it appears that As_2 is a better choice for limiting In segregation. Therefore, cracked As_4 should be employed.

- The simulated In composition versus growth monolayer number shows that the In segregation for substrate temperature range 803-903°K, starts at the 4^{th} monolayer and increases by increasing the number of layers.

- For lower As BEP, In segregation occurs at lower temperatures.

4.3 Advantages and limitations of the model

The kinetic rate equation model developed calculates the change in concentration of elements in each epilayer grown at each interval of time. Since the model is de-

scribed by a system of differential equations, the calculations can be performed at easily with less computational time. The model considers surface kinetic processes like incorporation, evaporation, migration, deposition, nucleation, growth of islands and interlayer and intralayer migration of atoms from the islands. The model is simple and not limited by crystal size. The doping kinetics in the crystal growth can be performed with ease. Any number of elemental sources can be considered with all surface processes applicable.

The main disadvantage of the model is that the microscopic details of the atoms such as size and shape of the islands cannot be obtained. The position of atoms or the energy cannot be determined and hence the sites available for antisites are considered only from the total number of atoms in the layer. The activation energies for evaporation, E_e and migration, E_d considered with four neighbor atoms is only approximate and may not exactly have neighbors as assumed. Those energies may be a different function of the coverage of atoms.

Table I Model parameters obtained by fitting the simulation results to the experimental data of Luysberg *et al.* [8] and obtained from Ref.[18].

Parameter	Description	Model Value
$\tau_{o,in}^{As_{Ga}}$	prefactor for antisite adsorption	172.0 s
$\tau_{o,ev}^{Phy,As}$	prefactor for physisorbed As evaporation	2.1x 10^{-4}
$\tau_{o,in,re}^{Phy,As}$	prefactor for physisorbed As incorporation in regular As site	172.0 s
$E_{d,iso}{}^{Ga}$	activation energy for diffusion for isolated Ga atom	0.4eV
$E_{d,iso}{}^{As_{Ga}}$	activation energy diffusion for isolated As_{Ga} atom	1.45eV
$E_{d,iso}{}^{As}$	activation energy for diffusion for isolated As atom	0.8eV
$E_{e,iso}{}^{Ga}$	activation energy for evaporation for isolated Ga atom	1.4eV
$E_{e,iso}{}^{As_{Ga}}$	activation energy diffusion for isolated As_{Ga} atom	1.3eV
$E_{e,iso}{}^{As}$	activation energy for diffusion for isolated As atom	1.5eV
E_{Ga-Ga}	2^{nd} neighbor atom-atom pair interaction energy for Ga	0.14eV
E_{As-As}	2^{nd} neighbor atom-atom pair interaction energy for As	0.25eV
$E_{As-As_{Ga}}$	2^{nd} neighbor atom-atom pair interaction energy for As and As_{Ga}	0.25eV
$R_0{}^{d,Ga}$	frequency factor for Ga for diffusion	2537.0/s.
$R_0{}^{e,Ga}$	frequency factor for Ga for evaporation	463970.0/s.
$R_0{}^{d,As_{Ga}}$	frequency factor for As_{Ga} for diffusion	7.8 x $10^{14}/s$.
$R_0{}^{e,As_{Ga}}$	frequency factor for As_{Ga} for evaporation	1.1 x $10^{12}/s$.
$R_0{}^{As}$	frequency factor for As	4.16 x 10^{10}/s.

Table II Fitted model parameters such as energies, time constants and frequency factors and their dependences for $InGaAs$

Symbol	Description	Model Value
$\tau_{0,in}^{Phy,Ga}$	prefactor for physisorbed Ga incorporation	10^{-3}s
$\tau_{0,in}^{Phy,As}$	prefactor for physisorbed As incorporation	10.0 s
$\tau_{0,in}^{Phy,In}$	prefactor for physisorbed In incorporation	0.2 s
$\tau_{0,ev}^{Phy,Ga}$	prefactor for physisorbed Ga evaporation	100.0s
$\tau_{0,ev}^{Phy,As}$	prefactor for physisorbed As evaporation	10^{-4}s
$\tau_{0,ev}^{Phy,In}$	prefactor for physisorbed In evaporation	10^{3}s
$R_0^{d,Ga}$	frequency factor for Ga for diffusion	2.4 X 10^{8}/s.
$R_0^{d,As}$	frequency factor for As for diffusion	4.38 X 10^{7}/s.
$R_0^{d,In}$	frequency factor for In for diffusion	4.38 X 10^{5}/s.
E_{in}^{Ga}	activation energy for incorporation of Ga	0.0 eV
E_{in}^{As}	activation energy for incorporation of As	1.0 eV
E_{in}^{In}	activation energy for incorporation of In	0.5 C_{In}^{phy} eV
E_{Ga-Ga}	2^{nd} neighbor atom-atom pair interaction energy for Ga	0.188 eV
E_{As-As}	2^{nd} neighbor atom-atom pair interaction energy for As	0.188 eV
E_{Ga-In}	1^{st} neighbor atom-atom pair interaction energy for Ga-In	0.0 eV
E_{In-In}	2^{nd} neighbor atom-atom pair interaction energy for In	0.173 eV
E_{Ga-As}	1^{st} neighbor atom-atom pair interaction energy for Ga-As	0.94 eV
E_{In-As}	1^{st} neighbor atom-atom pair interaction energy for In-As	0.86 eV
$E_{d,iso}^{Ga}$	activation energy for diffusion for isolated Ga atom	1.2 eV
$E_{d,iso}^{In}$	activation energy for diffusion for isolated In atom	1.3 eV
$E_{d,iso}^{As}$	activation energy for diffusion for isolated As atom	1.2 eV
$E_{e,iso}^{Ga}$	evaporation activation energy for isolated Ga atom	2.63 eV
$E_{e,iso}^{In}$	evaporation activation energy for isolated In atom	2.13 eV
$E_{e,iso}^{As}$	evaporation activation energy for isolated As atom	2.63 eV
E_{ev}^{Ga}	activation energy for the Ga evaporation	0.18+0.06$C_{Ga}^{phy^{*}}$ eV
E_{ev}^{In}	activation energy for the In evaporation	0.18+0.06$C_{In}^{phy^{**}}$ eV
E_{ev}^{As}	activation energy for the As evaporation	0.18+0.06$C_{As}^{phy^{***}}$ eV
$E_{s,In,iso}$	segregation activation energy for the isolated In atom	2.1 eV

$*$ C_{Ga}^{phy}-Ga coverage in the physisorbed layer
$**$ C_{In}^{phy}-In coverage in the physisorbed layer
$***$ C_{As}^{phy}-As coverage in the physisorbed layer

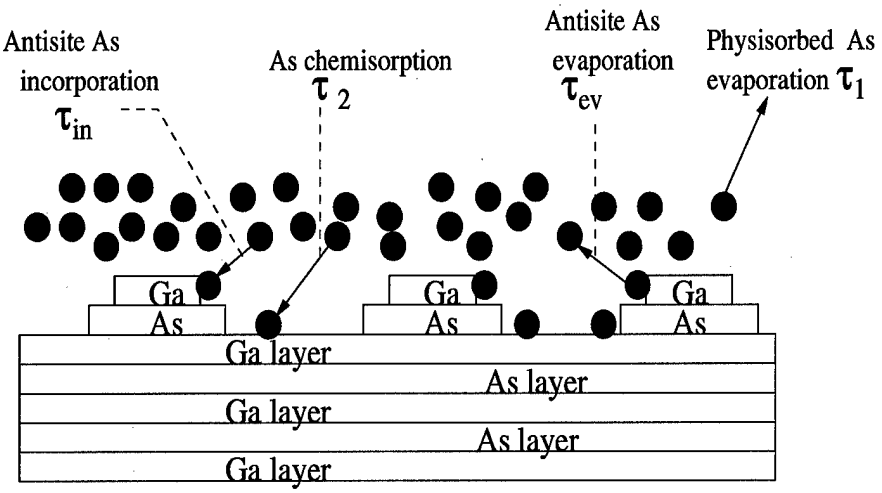

Figure 4.1: A schematic picture showing the surface processes of the physisorbed and antisite *As*.

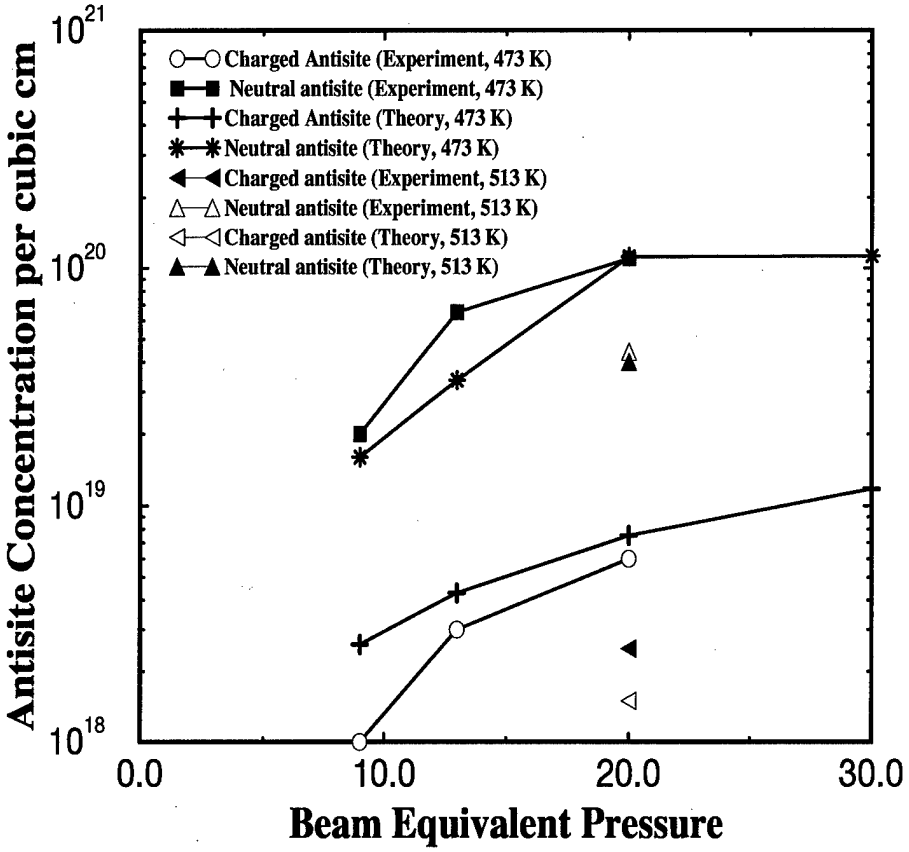

Figure 4.2: A plot of model results of charged and neutral antisite concentrations versus BEP along with the experimental results of Luysberg *et al* [8]

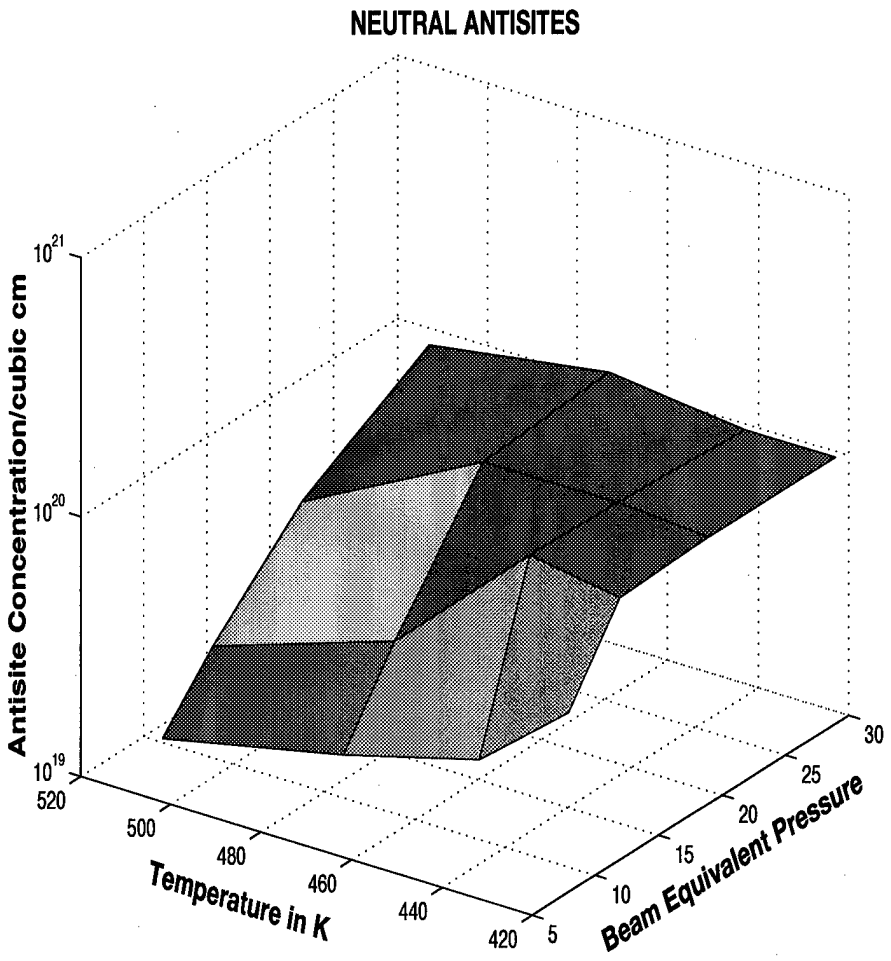

Figure 4.3: Model results of neutral antisites concentration versus BEP and Temperature.

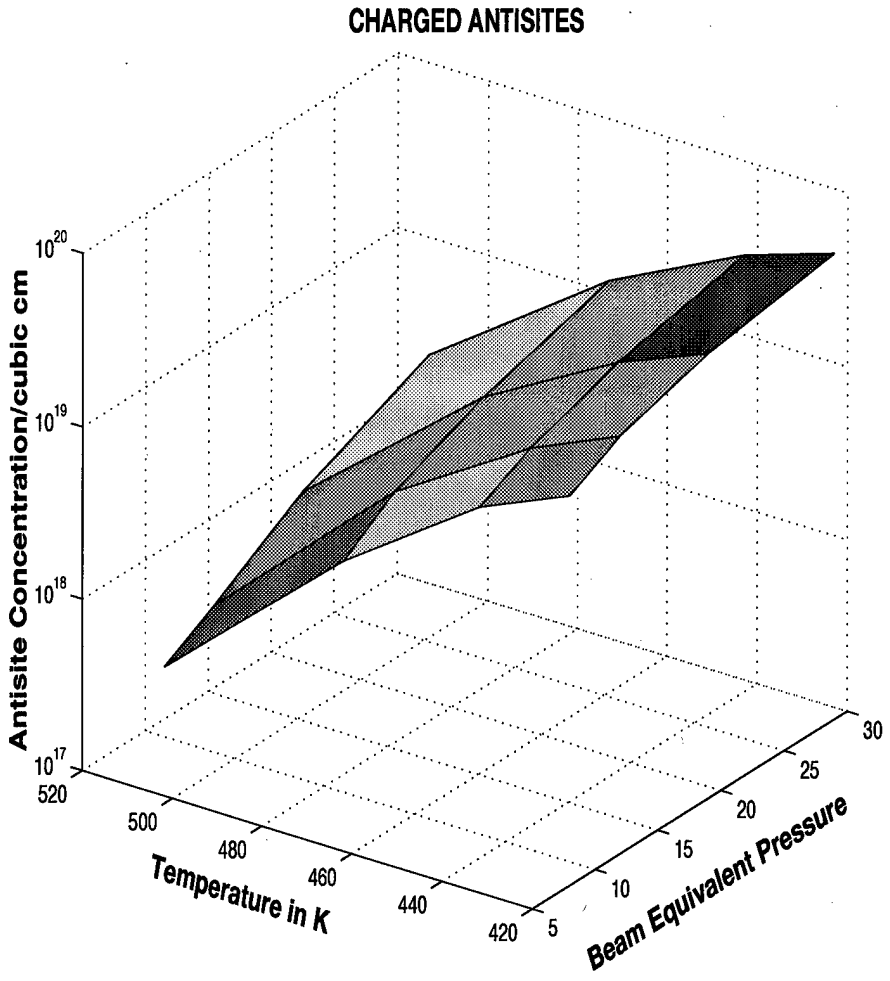

Figure 4.4: Model results of charged antisites concentration versus BEP and Temperature.

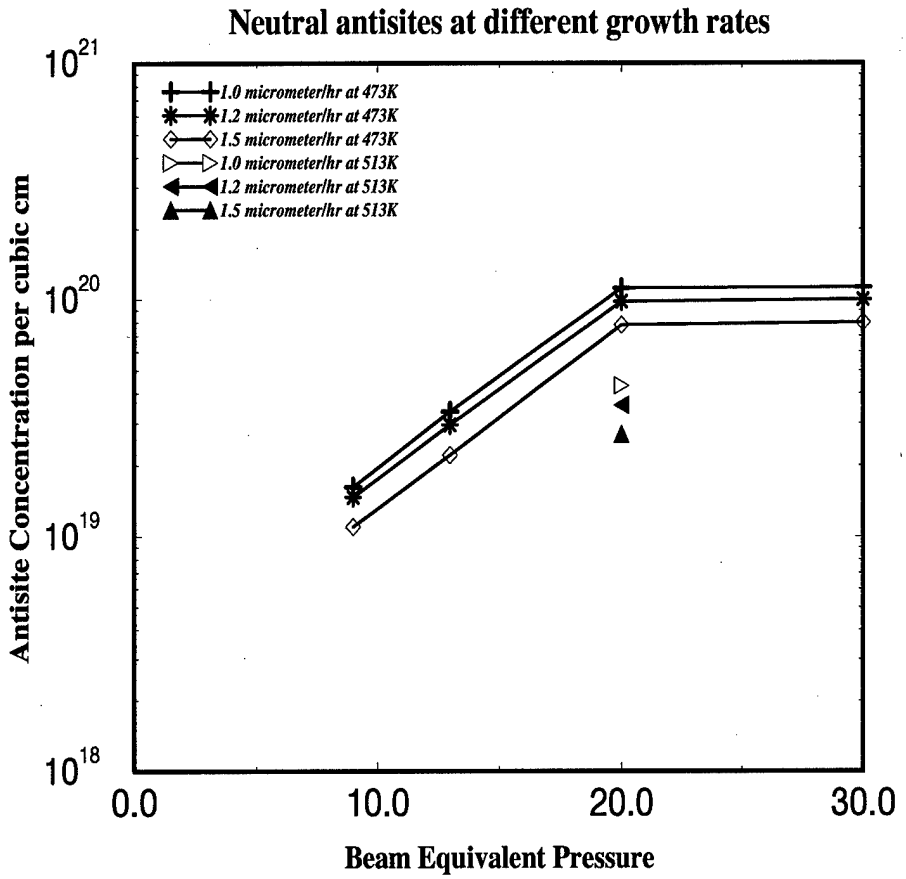

Figure 4.5: Model results of neutral antisites concentration versus BEP at different growth rates.

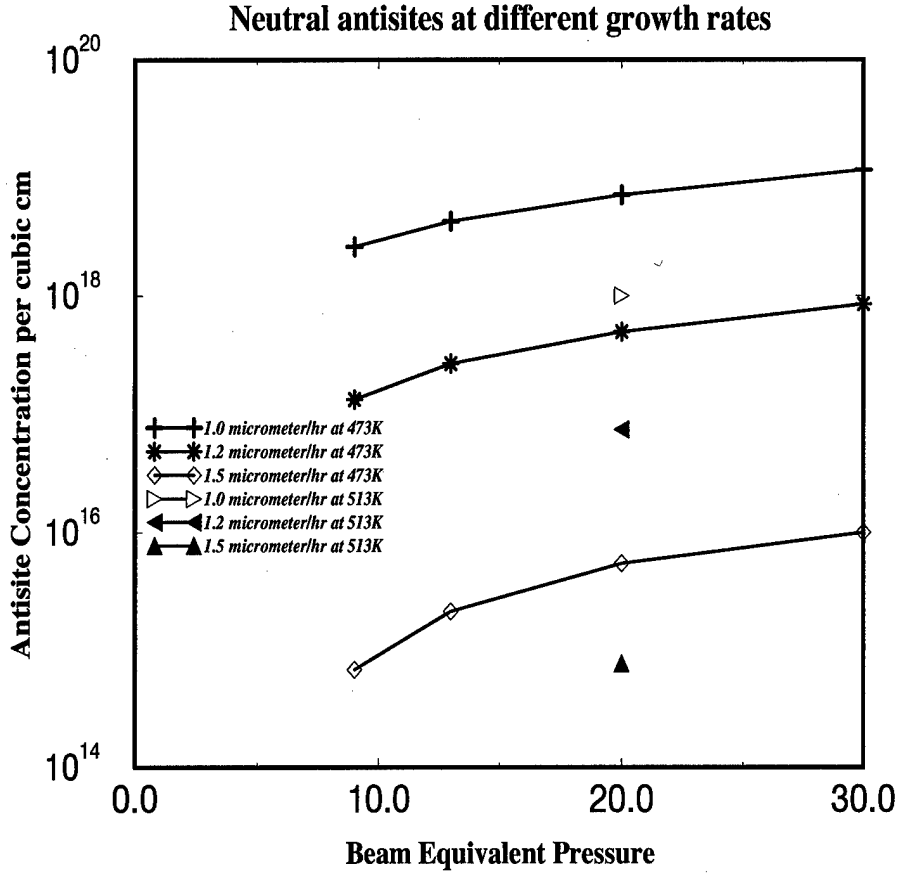

Figure 4.6: Model results of charged antisites concentration versus BEP at different growth rates.

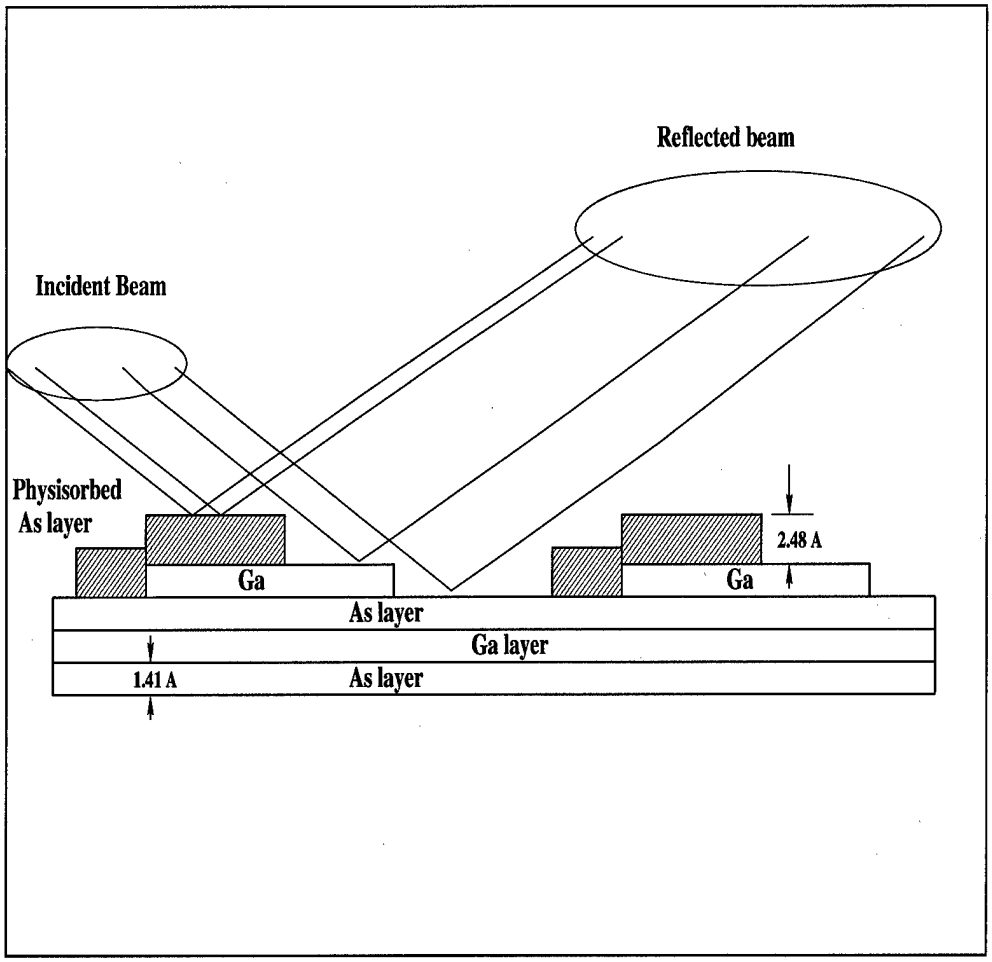

Figure 4.7: A schematic picture showing the reflected electron beams from the PA layer and the crystalline surface and the thicknesses of the layers.

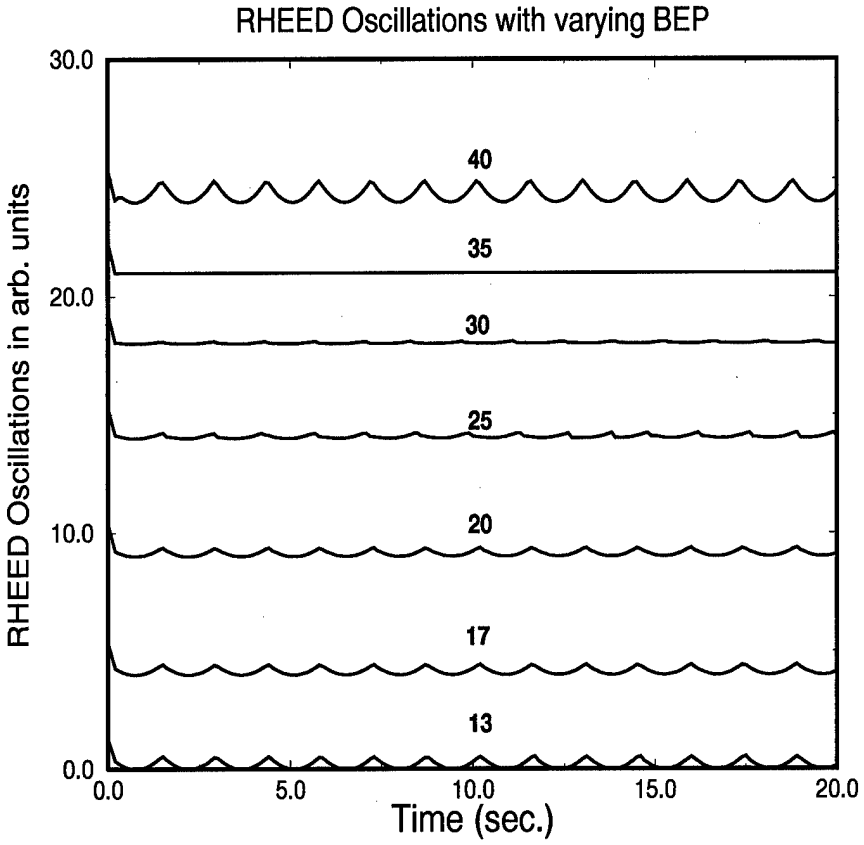

Figure 4.8: ROs versus time at 573°K for various BEP ratios at a growth rate of 0.7μm/hr. compared qualitatively with the experimental results of Shen *et al* : Fig. 1 of Ref.[18]

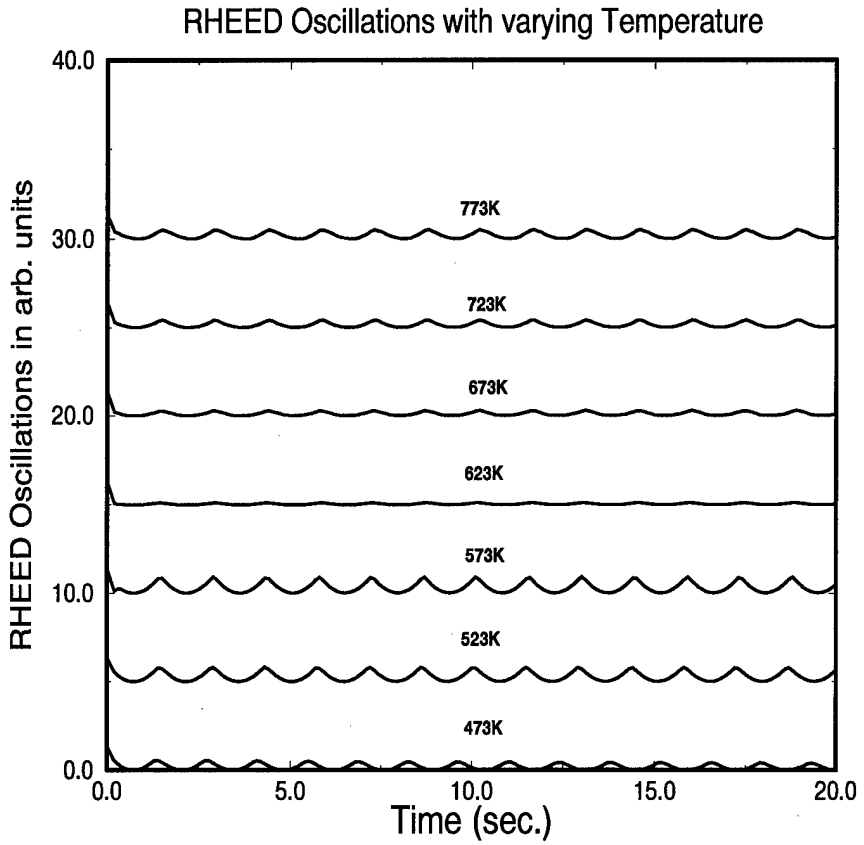

Figure 4.9: ROs versus time at 40 BEP for various temperatures at a growth rate of 0.7μm/hr. compared qualitatively with the experimental results of Shen *et al* : Fig. 3 of Ref. [18]

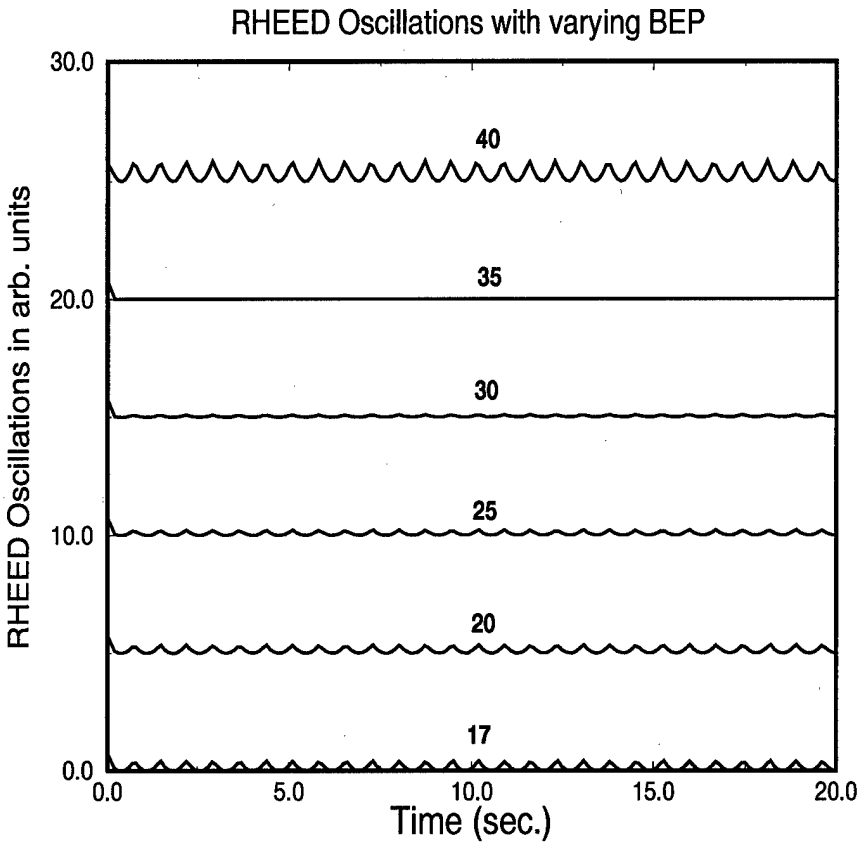

Figure 4.10: Model results of ROs versus time at 573°K for various BEP ratios at a growth rate of 1.4μm/hr.

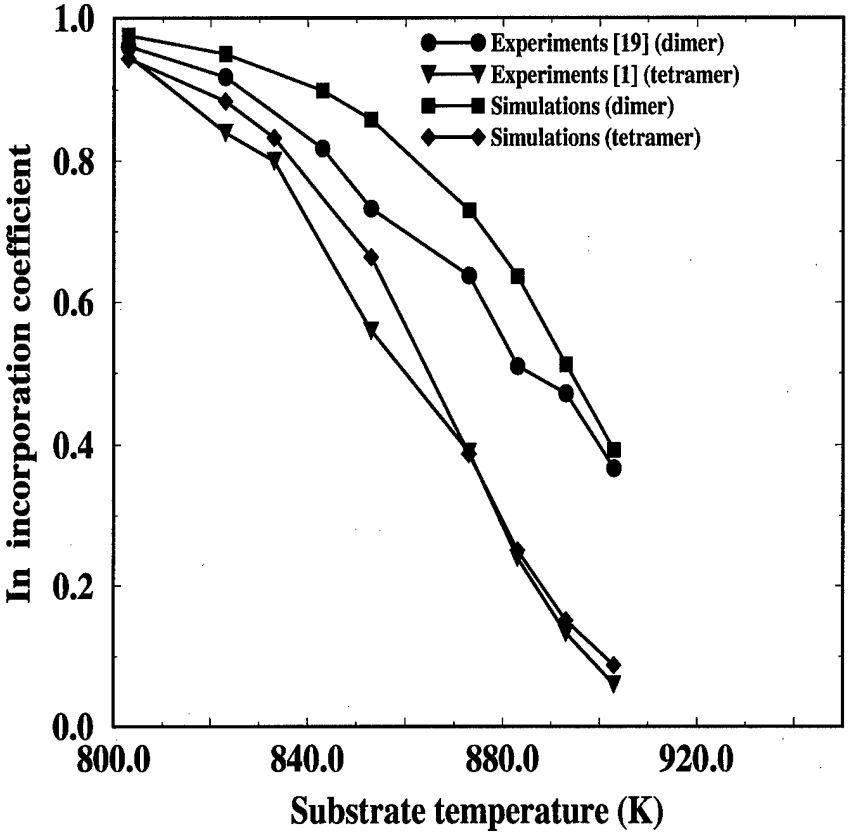

Figure 4.11: Comparison between experiments[19] and simulation results for In incorporation coefficient versus substrate temperature a BEP of 36 with As_2 and As_4 fluxes.

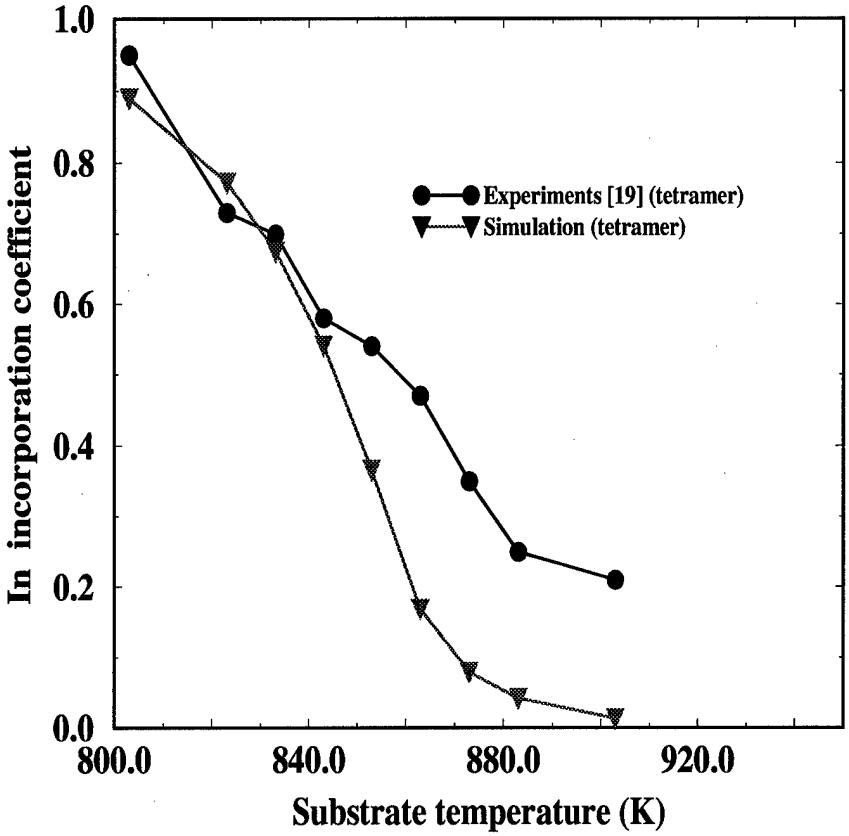

Figure 4.12: Comparison between experiments[19] and simulation results for In incorporation versus substrate temperature for a As_4 BEP of 17.

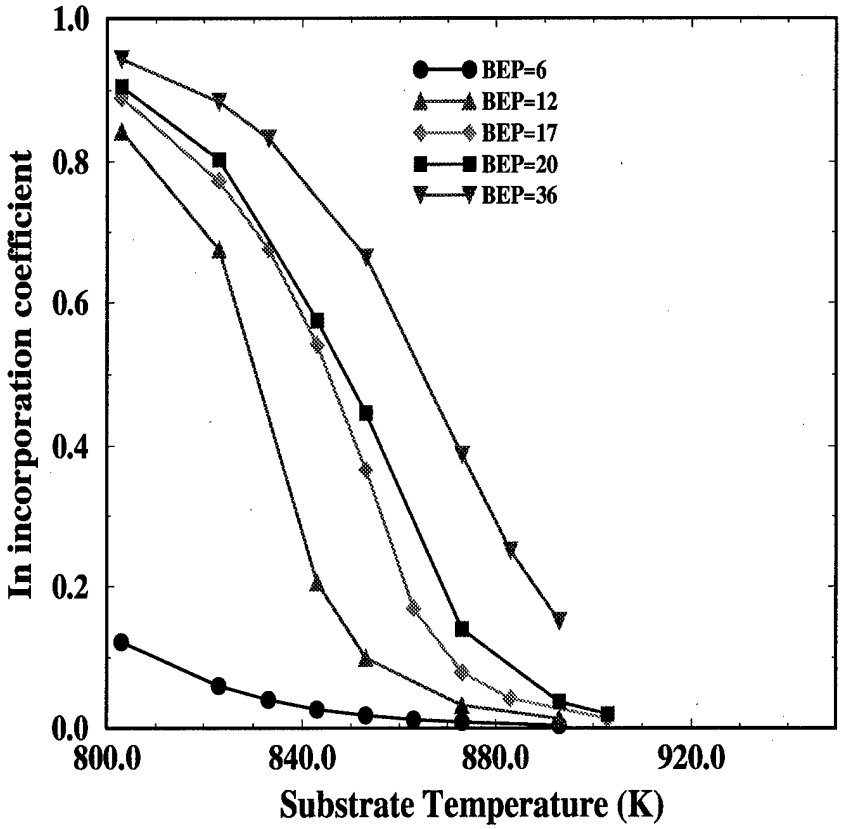

Figure 4.13: Simulation results of Indium incorporation versus substrate temperatures for various As_4 BEPs.

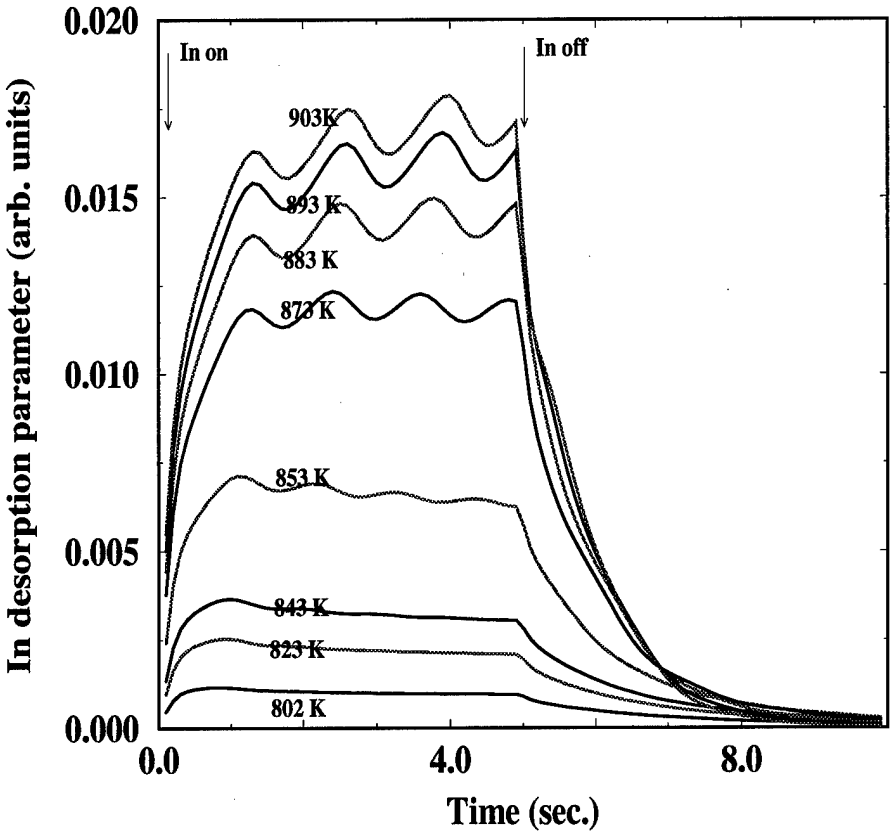

Figure 4.14: Simulation results of Indium desorption rate versus time for various substrate temperatures for a As_4 BEP of 36 for $803 < Ts < 903$ K.

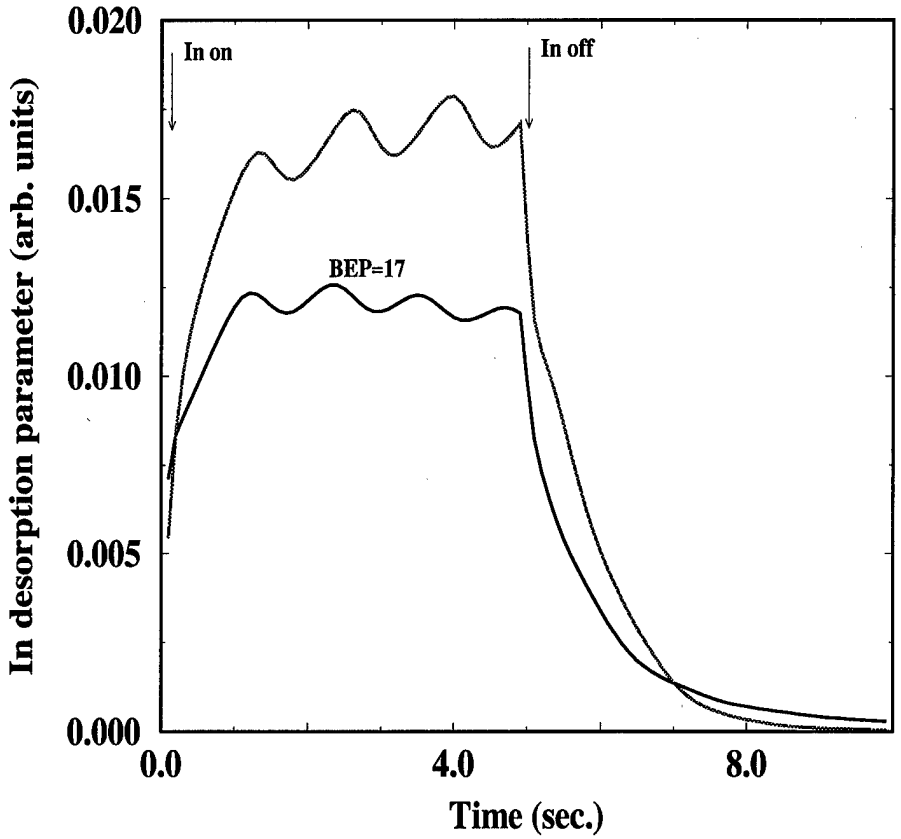

Figure 4.15: Simulation results of Indium desorption rate versus time for substrate temperatures 903°K for a As_4 BEP of 36 and 17.

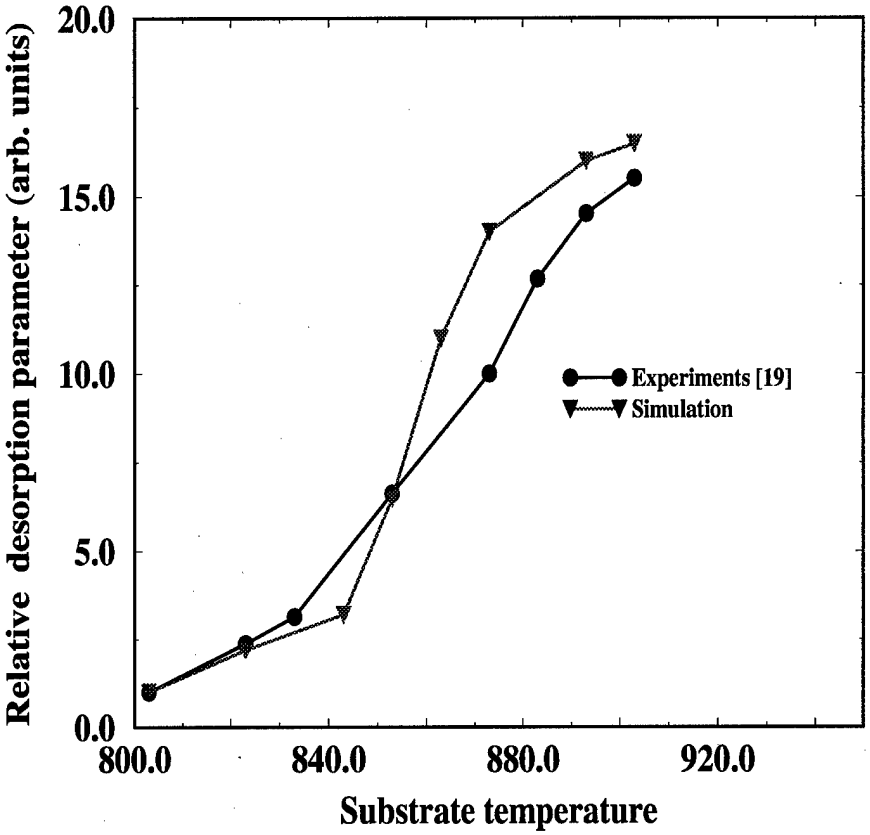

Figure 4.16: Comparison of simulation and experimental results [19] for relative desorption parameters of Indium versus substrate temperature for a As_4 BEP of 36 .

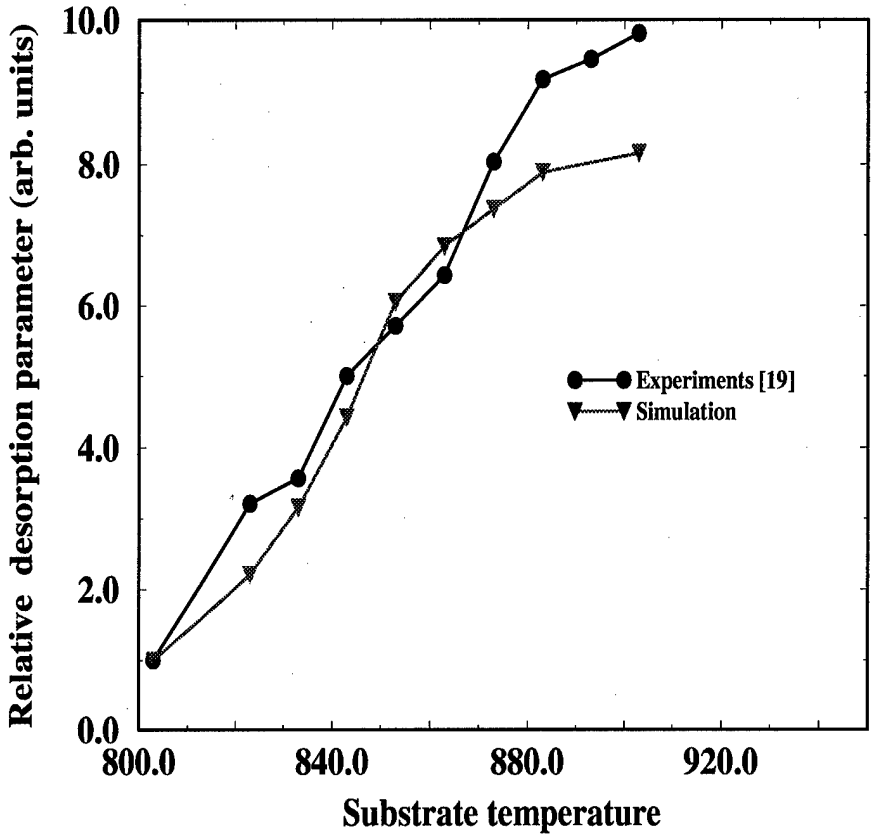

Figure 4.17: Comparison of simulation and experimental results [19] for relative desorption parameters of Indium versus substrate temperature for a As_4 BEP of 17.

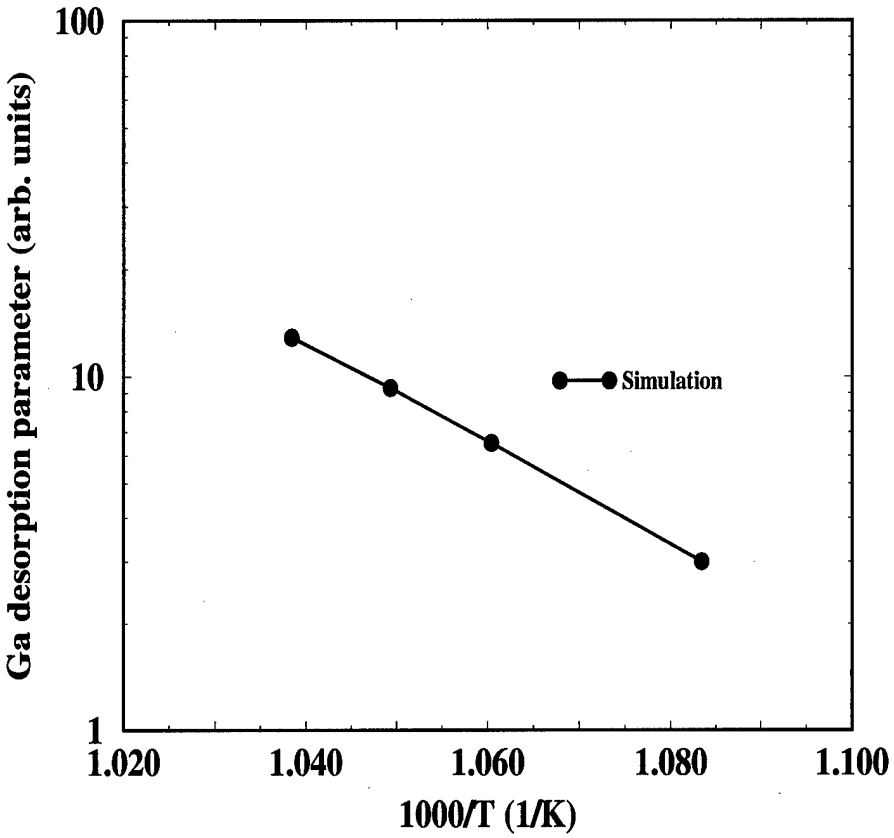

Figure 4.18: Simulation results of Ga desorption rate versus inverse of substrate temperature.

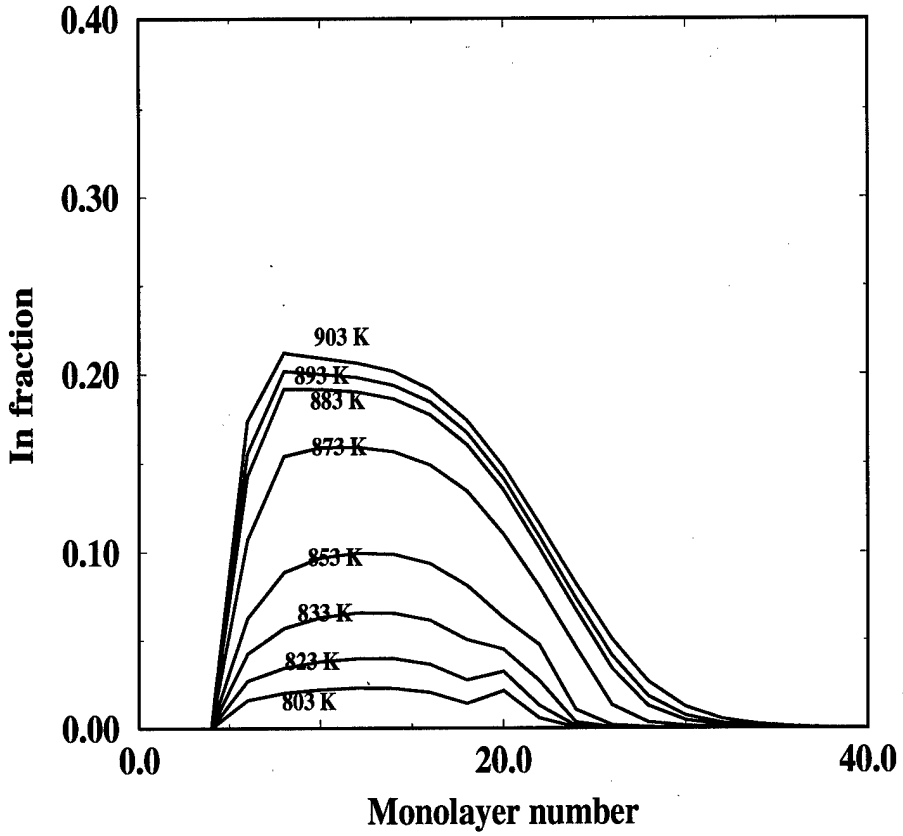

Figure 4.19: Simulation results of Indium composition versus monolayer number for various substrate temperatures for a As_4 BEP of 36 for 10 seconds growth.

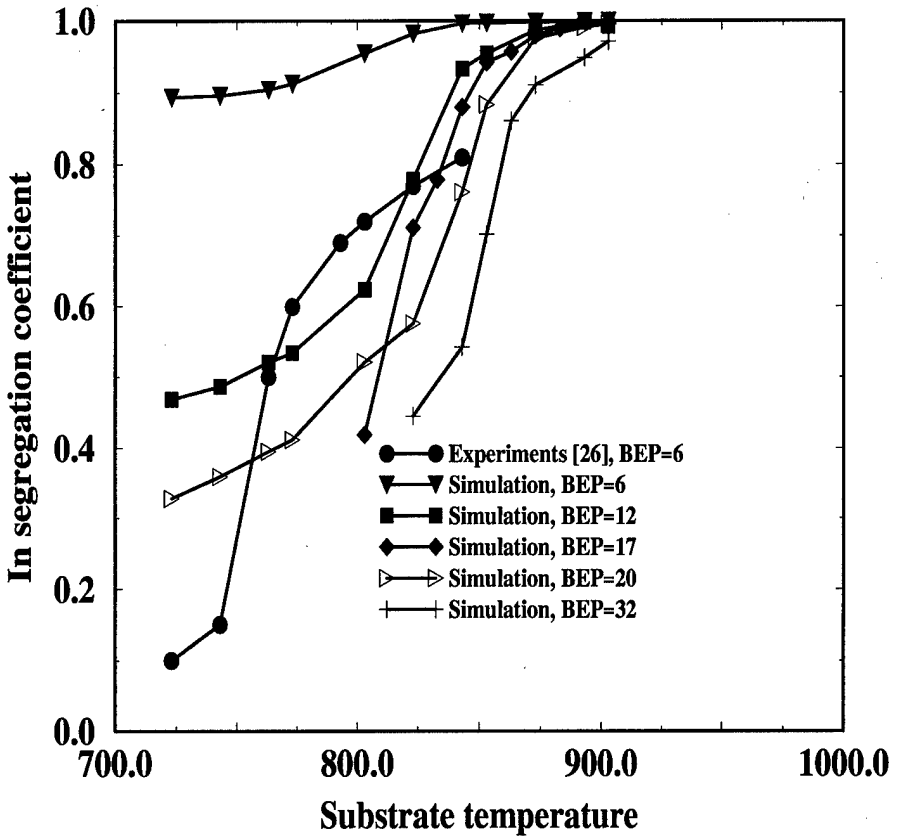

Figure 4.20: Simulation results of Indium segregation versus substrate temperatures for various As_4 and As_2 BEPs along with the experimental data of Kao *et al* [26] for a BEP of 6.

4.4 CURRENT EFFORT UNDERWAY

Currently, there is one growth simulation project underway, III-nitride growth using ammonia. As part of DEPSCoR 99, this work will be extended to cover ECR-plasma growth also.

4.5 PERSONNEL SUPPORTED

Name	Category	Period
Rama Venkat	Faculty	1 June, 1996 - 31 July, 1998
Muth Sivakumar	Graduate Student	1 June, 1996 - 31 May, 1997
Suresh Gorantla	Graduate Student	1 June, 1996 - 31 July, 1996
Yong Wang	Graduate Student	1 January, 1998 - 31 May, 1998
Krishnan Natarajan	Graduate Student	1 January, 1997 - 31, July, 1998
Wenning Fu	Graduate Student	1 August, 1998 - 31, June, 1999
Gulshan Colayni	Graduate Student	1 August, 1998 - 31, June, 1999

4.6 PUBLICATIONS

Three M.S. theses are completed and one more is in progress.

1. Muthuvenkatraman Sivakumar, M.S. degree, "*Antisite Incorporation in the Low Temperature Molecular beam Epitaxy of Gallium Arsenide* " September, 1997.

2. Natarajan Krishnan, M.S. degree, "*Low Temperature Molecular Beam Epitaxy of GaAs: Antisite Incorporation and RHEED Oscillations - A Theoretical Study*" September, 1998.

3. Gulshan Colayni, M.S. degree, "*Segregation and Desorption Studies in MBE of InGaAs: A Theoretical Study* " September, 1999.

4. Wenning Fu, M.S. degree, "*III-V Nitride MBE Growth Simulation*" Expected in May, 2000.

Several journal/conference proceedings articles were published.

1. S. Muthuvenkatraman, S.Gorantla, R. Venkat and D.L.Dorsey "*Antisite Incorporation in the Low Temperature MBE of GaAs: Physics and Modeling* " J. Electronic Materials, vol. 27, pp.472-478, 1998.

2. S.Muthuvenkatraman, S.Gorantla, R. Venkat and D.L. Dorsey, "*Theoretical Study of Antisite As incorporation in the Low Temperature MBE of GaAs*", Journal of Applied Physics, vol. 83, pp.5845-5851, 1998.

3. K.Natrajan, R.Venkat and D.L.Dorsey, "*Low Temperature molecular beam epitaxy of GaAs: A Theoretical investigation of antisite incorporation and reflection high energy electron diffraction oscillations*", J. Vac. Sci. Technol., vol. B17(3), pp.1227-1232, 1999.

4. K.Natrajan, R.Venkat and D.L.Dorsey, "*Low Temperature MBE of GaAs: A Theoretical investigation of RHEED oscillations*", J. Electronic Materials, vol. B28(7), pp.926-931, 1999.

5. Golshan Colayni and Rama Venkat, "*Growth Dynamics of InGaAs by MBE: Process Simulation and Theoretical Analysis*" accepted for publication in J. Crys. Growth, September, 1999.

6. K. Natrajan, R.Venkat and D.L.Dorsey, "*Influence of Growth Conditions on the As antisites, As^0_{Ga} and As^+_{Ga} concentrations in the Low Temperature GaAs MBE Growth: A First Theoretical Study*", Proceedings of 1998 IEEE Semiconducting and Insulating Materials Conference-X, June, 1998, pp.109-112.

Several Conference Presentations were made.

1. Muthuvenkraman Sivakumar, R.Venkat and D.L.Dorsey, "*Antisite Arsenic Incorporation in the Low Temperature MBE of Gallium Arsenide: Physics and Modeling*, presented at the 39^{th} Electronic Materials Conference, Fort Collins, June, 1997.

2. K.Natraj, R.Venkat and D.L.Dorsey, "*Influence of Growth Conditions on the antisite As^0_{Ga} and As^+_{Ga} concentrations in the Low Temperature GaAs MBE Growth: A First Theoretical Study*" presented at SIMC-X conference, Berkeley, June, 1998.

3. K.Natraj, R.Venkat and D.L.Dorsey, "*Low Temperature MBE of GaAs: A Theoretical investigation of RHEED oscillations*", presented at the Tenth International Conference on MBE at Cannes, France, September, 1998.

4. K.Natraj, R.Venkat and D.L.Dorsey, "*Low Temperature molecular beam epitaxy of GaAs: A Theoretical investigation of antisite incorporation and reflection high energy electron diffraction oscillations*" presented at the Seventeenth North American Conference on MBE at Pennsylvania State University, October, 1998.

5. Gulshan Colayni and Rama Venkat, "*Growth Dynamics of InGaAs by MBE: Process Simulation and Theoretical Analysis*" submitted to the 18^{th} ACCGE-11, Tucson, August, 1999.

6. Wenning Fu and Rama Venkat, "*theoretical study of GaN Growth Using Ammonia: A Rate Equation Approach*" accepted for presentation in the 18^{th} North American Molecular Beam Epitaxy Conference, Banff, 1999.

Several Proposals were submitted and and one was funded by AFOSR.

1. Several proposals related to the project were submitted to federal funding agencies such NSF, AFOSR, WPAFB and DOE.

2. R. Venkat, "*Molecular beam Epitaxy of Nitrides: Theoretical Modeling and Process Simulation*", submitted to DEPSCOR/AFOSR, $252,200, 1998 (**Funded**).

4.7 INTERACTIONS

Our ongoing collaboration with Dr. Weber's group of University of California, Berkeley is flourishing very well. We interact with their group sharing results, ideas and comments. We are currently trying to establish collaborations other groups from around world searching for systematic experimental data of LT MBE of III V compounds. Dr. Dorsey of Materials Directorate, WPAFB has provided theoretical support throughout the course of the project.

4.8 NEW DISCOVERIES, INVENTIONS AND PATENTS

Most of discoveries have been theoretical ones.

1. Both charged and neutral antisite concentrations saturate with BEP for a given temperature.

2. Charged antisite As concentration versus temperature is linearly decreasing due to decreasing Ga vacancy concentration with temperature.

3. There is a temperature and BEP window within which, there is no RHEED oscillations and outside of which there is RHEED oscillations. This effect is attributed to the presence and contribution to the scattered electron beam of a As physisorbed layer riding the surface.

4. The In segregation rate is large for higher temperature and low As overpressure. Thus, to minimize the In segregation, one should adopt lower temperatures and high As over-pressures. But, the temperature should not so low that the other thermally activated surface processes such as migration and As molecular adsorption by reaction are suppressed.

5. As_2 limits In segregation rate more compared to As_4 of the same BEP. It appears that As_2 is a better choice for limiting In segregation. Therefore, cracked As_4 should be employed.

6. *In* desorption has two components, one from the surface riding *In* layer and the other from the surface of the crystal itself. The former component is smaller than the latter.

7. A general kinetic rate equation model which applies to MBE growth of most compound semiconductors is developed. The only difference among these models for various systems is the system-specific model parameters.

4.9 HONORS AND AWARDS

None.

BIBLIOGRAPHY

[1] T. Murotani, F. Shimanoe and S.Mitsui, *J. Cryst. Growth* **45**, 302 (1978).

[2] Melloch M.R., Otsuka N., Woodall J.M., Warren A.C., and Freeouf J.L., *Appl. Phys. Lett.*, **57**, 1531 (1990).

[3] F. W. Smith, A. R. Calawa, C. L. Chen, M. J. Manfra and L.J. Mahoney, *IEEE Electron Device Lett. EDL* **9**, 77 (1987).

[4] Kaminska M., Weber E.R., Liliental-Weber Z., Leon R., Rek ZU., *J. Vac. Sci. Technol*, **B7**, 943 (1989).

[5] D.Keeble, M.T.Umlor, P.Asoka-Kumar, K.G.Lynn and P.W.Cooke, *Appl. Phys. Lett.*, **83**, 87 (1993).

[6] Z.Liliental-Weber, J.Ager, D.Look, X.W.Lin, X.Liu, J.Nisho, K.Nichols, W.Schaff, W.Swider, K.Wang, J.Washburn, E.R.Weber and J.Whitaker, in: *Proc. of the* 8^{th} *Conf. on Semiinsulating III-V Materials, ed. M Godlewski(World Scientific, 1994)* p.305.

[7] X.Liu, A. Prasad, W.M. Chen, A. Kurpiewski, A.Stoschek, E.R. Weber, Z. Liliental-Weber, *Appl. Phys. Lett.*, **65**, 3002 (1994).

[8] M. Luysberg, H. Sohn, A. Prasad, P. Specht, Z. Liliental-Weber, E.R. Weber, J. Gebauer and R. Krause-Rehberg, *J. Appl. Phys.*,, **83**, 561 (1998).

[9] P. Specht, S. Jeong, H. Sohn, M. Luysberg, A. Prasad, J. Gebauer, R. Krause-Rehberg, E.R. Weber, *Proceedings of the Int. Conf. on Defects in Semiconductors ICDS 19, Aveiro, Portugal, Mater. Sci. Forum*, **258-263**, 951 (1997).

[10] S. Muthuvenkatraman, Suresh Gorantla, Rama Venkat, Donald L. Dorsey, *J. Elec. Matrls.*, **27/5**, 472 (1998).

[11] Neave J.H., Dobson P.J., Joyce B.A., and Zhang, *Appl. Phys. Lett.*, **47**, 100 (1985).

[12] Van Hove J.M., Lent C.S., Pukite P.R., and Cohen P.I, *J. Vac. Sci. Technol. B*, **3**, 563 (1985).

[13] C.E.C. Wood, *Surf, Sci.*, **108**, L441 (1981).

[14] J.J. Harris, B.A. Joyce, *J. Cryst. Growth*, **44**, 387 (1978).

[15] Ibbetson J.P., Mirin R.P., Mishra U.K. and Gossard A.C., *J. Vac. Sci. Technol. B*, **12**, 1050 (1994).

[16] Richard P.Mirin, James P.Ibbetson, Umesh K.Mishra and Arthur C.Gossard, *Appl. Phys. Lett.*, **65(18)**, 2335 (1994).

[17] R. Venkatasubramanian, Vamsee K. Pamula and Donald D. Dorsey, *Applied Surface Science*, **104/105**, 448 (1996).

[18] A. Shen, Y.Hiroshi, H.Ohno and S.P.Guo, Appl. Phys. Lett., vol. 71, (1997), p1540.

[19] Franciose Fournier, Robert A. Metzger and Alen Doolittle, *Journal of Crystal Growth*, **175/176**, 203, 1997.

[20] K.R Evans and C. Stutz, *J. Vac. Sci. Technol.*, **B 9**, 2427, 1991.

[21] J. Zhang and C. Foxon, *J. Crystal Growth*, **111**, 93, 1991.

[22] M. Mesrine, J. Massies and M. Leroux, *J. Crystal Growth*, **175/176**, 1242, 1997.

[23] K. Evans and C. Stutz, *J. Crystal Growth*, **95**, 197, 1989.

[24] K. Evans and R. Kaspi, J.E.Ehret, M.Skowronski and C.R. Jones, *J. Vac. Sci. Technol.*, **B 13**, 1820, 1995.

[25] R. Kaspi and K. Evans, *Appl. Phys. Lett.*, **67**, 819, 1995.

[26] Y. Kao and F. Celli, *J. Vac. Sci. and Technol.*, **B 11**, 1023, 1993.

[27] K. Muraki and S. Fukatsu, *Appl. Phys. Lett.*, **61**, 557, 1992.

[28] Karl Woodbridge, *Appl. Phys. Lett.*, **60**, 2911, 1992.

[29] K. Evans and C. Stutz, *Appl. Surf. Sci.*, **56-58**, 677, 1992.

[30] Jean-Michel Gerard, *J. Crystal Growth*, **150**, 467, 1995.

[31] K Radhakrishnan and S. Yoon, *J. Vac. Sci. and Technol.*, **A 12**, 1124, 1994.

[32] H. Toyoshima and T. Niwa, *Appl. Phys. Lett.*, **63**, 821, 1993.

[33] C. Foxon and B. Joyce, *J. Crystal Growth*, **44**, 75, 1978.

[34] Teruo Mozume and Isao Ohbu, *J. J. Appl. Phys.*, **31**, 3277, 1993.

[35] F.Houzay, J.M.Moison, C.Guille, F.Barthe and M. Van Rompay, *J. Crystal growth*, **95**, 1989, 35.

[36] M. Luysberg, H. Sohn, A. Prasad, P. Specht, Z. Liliental-Weber, E.R. Weber, J.Gebauer and R. Krause-Rehberg, IEEE SIMC-9., pp.21-26, 1996.

[37] A.Y. Cho and J.R. Arthur, *Prog. Solid State Chem.* **10**, 157 (1975).

[38] B.A. Joyce, *Rep. Prog. Phys.* **48**, 1637,1985

[39] K. Ploog, *Molecular bean epitaxy of III-V compounds, in Crystals-Growth, Properties and Applications*, Vol.3, ed. by H. C .Freyhardt (Springer, Berlin, Heidelberg 1980) p. 73.

[40] M. R. Melloch, D.D. Nolte, J. M. Woodall, N. Otsuka, Fred H. Pollak, E. S. Harmon, R. M. Feenstra and M. A. Lutz, *Ann. Rev. Mater. Sci.*, **25**, 547-600 (1995).

[41] R.F.C. Farrow, *J. Phys. D*, **7**, L 121 (1974).

[42] R.A. Stall, C.E.C. Wood, P.D. Kirchner and L.F. Eastman, *Electron Lett.*, **16**, 171 (1980).

[43] D.J. Eaglesham, L.N.Pfeiffer, K.W. West, D.R. Dykaar, *Appl. Phys. Lett.*, **58**, 65 (1991).

[44] G.M.Metze and A.R.Calawa, Appl. Phys. Letts., **42**, 9, (1983)

[45] M.J.Delaney, C.S. Chou, L.E. Larson, J.F. Jensen, D.S. Deakin, A.S. Brown, W.W. Hooper, M.A. Thompson, M.G. McCray and S.C. Rosenbaum, *IEEE Electron Device Lett.*, **10**, 355 (1989).

[46] L.W. Yin, Y. Hwang, J.H. Lee, R.M. Kolbas, R.J. Trew and U.K. Mishra, *IEEE Electron Device Lett.*, **12**, 306 (1991).

[47] M.R. Melloch, D.C. Miller, B. Das, *Appl. Phys. Lett.*, **54**, 943 (1989).

[48] B.J.F. Lin, C.P.Kocot, D.E. Mars, R. Jaeger, *IEEE Electron Devices*, **37**, 46 (1990).

[49] P.M. Solomon, S.L. Wright, F.J. Canora, *IEEE Electron Device Letts.*, **12**, 117 (1991).

[50] G. Subramanian, A. Dodabalapur, J.C. Campbell, B.G. Streetman, *Appl. Phys. Letts.*, **58**, 2514 (1991).

[51] T.J. Rogers, C. Lei, B.G. Streetman, D.G. Deppe, *J. Vac. Sci. Technol. B*, **11**, 926 (1993).

[52] A. Rahman, D. Kralj, L. Carin, M.R. Melloch, J.M. Woodall, *Appl. Phys. Lett.*, **64**, 2178 (1994).

[53] R.J. Matyi, M.R. Melloch, J.M. Woodall, *J. Crys. Growth*, **60**, 2642 (1992).

[54] K. Mahalingam, N. Otsuka, M.R. Melloch, J.M. Woodall, A.C. Warren, *J. Vac. Sci. Technol.B*, **9**, 2328 (1991).

[55] M.R. Melloch, N. Otsuka, K. Mahalingam, C.L. Chang, J.M. Woodall, *J. Appl. Phys.*, **72**, 3509 (1992).

[56] D.C. Look, D. C. Walters, M. Mier, *Appl. Phys. Lett.*, **60**, 2900 (1990).

[57] Gebauer, Weber, *Appl. Phys. Lett.*, (1997).

[58] N.Hozhabri, S.H. Lee and K. Alavi, *Appl. Phys. Lett.*, **66**, 2456, (1995).

[59] S.B. Zhang and J.E. Northrup,*Phys.Rev. Lett.*,**67**, 2339, (1991).

[60] D.J .Chadi, *Phys.Rev. B*, **46**, 9400, (1992).

[61] A.C. Warren, J.M. Woodall, J.L. Freeouf, D. Grichkowsky, D.T. McIntuff, *Appl. Phys. Lett.*, **57**, 1331, (1990).

[62] J.P. Ibbetson, J.S. Speck, N.X. Nguyen, *J.Electron Mater.*, **22**, 1421, (1993).

[63] X.Liu, A.Prasad, J.Nishio, E.R. Weber, Z.Liliental-Weber, W.Walukiewicz, *Appl. Phys. Lett.*,**67**, 279, (1995).

[64] K.M. Yu, M. Kaminska and Liliental-Weber, *J. Appl. Phys.*, **72**, 2850 (1992).

[65] M.Lagadas, Z. Hatzopoulos, K. Tsagaraki, M. Calamiotou, C. Lioutas, A. Christou,*J. Appl. Phys.*,**80**(8), 4377 (1996).

[66] A.Y. Cho, *Thin solid films*, **100**, 291, (1983).

[67] M.A. Herman and H. Sitter, *Molecular Beam Epitaxy-Fundamentals and current status, Springer series in Material Science 7*, p145, (1996).

[68] J.J. Harris, B.A. Joyce and P.J. Dobson, *Surf. Sci.*,**103**, L90, (1981).

[69] G.S. Petrich, P.R. Pukite, A.M. Wowchak, G.J. Whaley, P.L. Cohen and A.S. Arrott, *J.Crystal Growth*, **95**,23, (1989).

[70] R.S. Resh, K.D. Jamison, J. Strozier, A. Bensaoula and Ignatiev, *J. Vac. Sci. Technol.* **41**, 1052, (1990).

[71] T. Shitara, D.D. Vvedensky, R. Wilby, J. Zhang, J.H. Neave and B.A. Joyce, *Phys.Rev. B*, **46**, 6825, (1992).

[72] J. Sudijono, M.D. Johnson, C.W. Snyder, M.B. Elowitz and B. Gorr, *Phys. Rev. Lett.*, **69**, 2811, (1992).

[73] A.M. Dabiran, P.I. Cohen, J.E. Angelo and W.W. Gerberich, *Thin solid films,* **231**, 1-7, (1993).

[74] A. Madhukar and S.V. Ghaisas, *Appl. Phys. Lett.*, **47**, 3 (1985).

[75] J. Singh and K.K. Bajaj, *J. Vac. Sci. Technol. B*, **3**, 520 (1985).

[76] S.V. Ghaisas and A. Madhukar, *J. Vac. Sci. Technol. B*, **7**(2), 264 (1989).

[77] S. Clark and D.D. Vvedensky, *J. Appl. Phys.*, **63**, 2272 (1988).

[78] K. Mahalingam, D.L. Dorsey, K.R. Evans, Rama Venkat, *Appl. Phys. Lett.*, **70**(23), 3143 (1997).

[79] B.W. Dodson and P.A. Taylor, *Phys. Rev. B*,**36**, 1355 (1987).

[80] H. Sitter, *Thin Solid Films*, **267**, 37 (1995).

[81] M. Schneider, I.K. Schuller and A. Rahman, *Phys. Rev. B*, **36**, 1340 (1987).

[82] R. Venkatasubramanian, *J. Mater. Res.*, **7**, 1221 (1992).

[83] R. Venkatasubramanian, *J. Mater. Res.*, **7**, 1236 (1992).

[84] Y. Saito and H.H. Krumbhaar, *J. Chem. Phys.*, **65**, 729 (1990).

[85] S. Muthuvenkatraman, Suresh Gorantla, Rama Venkat, Donald L. Dorsey, *J. Appl. Phys.*,**80**, 6219 (1996).

[86] R. Venkatasubramanian and D.L. Dorsey, *J. Vac. Sci. and Technol. B*, **11**, 253 (1993).

[87] Shridhar Bendi, R. Venkatasubramanian, D.L. Dorsey, *J. Appl. Phys.*, **76**,(9), 5202 (1994).

[88] F. H. Stillinger, T.A. Weber, *Phys. Rev. B*, **31**, 5262 (1985).

[89] C.T.Foxon and B.A.Joyce, *Surf. Sci.,* **64**, 293, 1977.

[90] C.T.Foxon and B.A.Joyce, *Surf. Sci.,* **50**, 434, 1975.

[91] T.B. Joyce and T.J. Bullough *J. Crystal Growth*,**127**, 265 (1993).

[92] Eicke Weber (private communication)